

Seasonal to Mesoscale Variability of Water Masses and Atmospheric Conditions in Barrow Canyon, Chukchi Sea

Robert S. Pickart^a, Carolina Nobre^a, Peigen Lin^a, Kevin R. Arrigo^b, Carin J. Ashjian^a, Catherine Berchok^c, Lee W. Cooper^d, Jacqueline M. Grebmeier^d, Ian Hartwell^e, Jianfeng He^f, Motoyo Itoh^g, Takashi Kikuchi^g, Shigeto Nishino^g, Svein Vagle^h

^a*Woods Hole Oceanographic Institution, Woods Hole, MA, USA*

^b*Department of Earth System Science, Stanford University, Stanford, CA, USA*

^c*Pacific Marine Environmental Laboratory, Seattle, WA, USA*

^d*University of Maryland Center for Environmental Science, Cambridge, MD, USA*

^e*National Oceanic and Atmospheric Administration, Silver Spring, MD, USA*

^f*Polar Research Institute of China, Shanghai, China*

^g*Japan Agency for Marine-Earth Science and Technology, Yokosuka, Kanagawa, Japan*

^h*Institute of Ocean Sciences, Sidney, British Columbia, Canada*

Abstract

Twenty-four repeat hydrographic transects occupied across Barrow Canyon from 2010 to 2013 are used to study the seasonal evolution of water masses in the canyon from July–October as well as the occurrence of upwelling. The mean sections revealed that the Alaskan coastal water is mainly confined to the eastern flank of the canyon, corresponding to a region of sloped isopycnals indicative of the surface-intensified Alaskan Coastal Current. The Pacific-origin winter water is found at depth, banked against the western flank of the canyon. Its isopycnal structure is consistent with a bottom-intensified flow of this dense water mass out of the canyon. For the months that were sampled, the Alaskan coastal water is most prevalent in August and September, while the coldest winter water is observed in the month of August. It is argued that this newly ventilated winter water is delivered to the canyon via pathways on the central Chukchi shelf, as opposed to the coastal pathway. Roughly a third of the hydrographic sections were preceded by significant up-canyon winds and hence were deemed to be under the influence of upwelling. During these periods, anomalously salty water is found throughout the eastern flank of the canyon, and, on occasion, Atlantic water fills the deepest part of the section. Using atmospheric reanalysis data it is shown that upwelling occurs when the Beaufort High is strengthened and the Aleutian Low is deepened. Two modes of storm tracks were identified: northward progressing storms (mode 1) and

31 eastward progressing storms (mode 2), both of which can drive upwelling. Mode 1 is prevalent
32 in July–August, while mode 2 is more common in September–October. These seasonal patterns
33 appear to be dictated by regional variations in blocking highs.

34 *Keywords:* Barrow Canyon; boundary currents; wind-forced upwelling

35 **1. Introduction**

36 Barrow Canyon is one of the primary conduits by which Pacific-origin water exits the Chukchi
37 Sea into the Canada Basin. Based on data from a long-term mooring array at the mouth of the
38 canyon, Itoh et al. (2013) calculated a mean northward transport of Pacific water of 0.44 Sv, which
39 is approximately 50% of the mean transport through Bering Strait over the same time period (cal-
40 culated using data from Woodgate et al., 2015). In the summer season this percentage seems to
41 be even larger. Several recent observational studies have estimated that up to 1 Sv of Pacific wa-
42 ter flows northward through the canyon during the summer months (Itoh et al., 2015; Gong and
43 Pickart, 2015; Pickart et al., 2016).

44 The water approaches the canyon via different flow pathways on the Chukchi shelf (Fig 1). The
45 coastal pathway, which in summertime is known as the Alaskan Coastal Current (ACC), provides
46 the fastest and most direct route for water to travel from Bering Strait to Barrow Canyon (Wein-
47 gartner et al., 1998). The other pathways are more circuitous and feed the canyon more slowly
48 (Winsor and Chapman, 2004; Spall, 2007). In particular, the Central Channel pathway divides into
49 filaments in the vicinity of Hanna Shoal (Weingartner et al., 2013; Pickart et al., 2016, Fig 1), and,
50 presumably, each of these filaments drains into Barrow Canyon. In addition, some of the water in
51 the western pathway is diverted eastward and joins the Central Channel branch (Weingartner et al.,
52 2005; Spall, 2007; Pickart et al., 2010). The timing by which the Pacific water in these interior shelf
53 pathways is delivered to the canyon is presently unknown, although it is clear that this is strongly
54 influenced by the wind (Winsor and Chapman, 2004).

55 The characteristics of the water masses that flow across the Chukchi shelf vary markedly with
56 season. In winter and early spring most of the shelf is filled with cold water near the freezing point
57 (Pacini et al., this issue), which is referred to as newly ventilated Pacific winter water (NVWW).

58 This water originates from the Bering Sea (Muench et al., 1988) and flows through Bering Strait,
59 but it is also formed and/or further modified on the Chukchi shelf (Weingartner et al., 1998; Itoh
60 et al., 2012). Later in the spring, warmer and fresher water flows through Bering Strait from
61 the central Bering shelf and the Gulf of Anadyr; north of the strait this mixture is referred to as
62 Bering summer water (BSW, e.g. Pisareva et al., 2015). During summer and early-fall, Alaskan
63 coastal water (ACW) flows northward on the eastern side of Bering Strait. This is the warmest and
64 freshest water that enters the Chukchi Sea, and it flows towards Barrow Canyon in the ACC. (At
65 times the ACW can be fluxed westward onto the interior shelf due to wind-forced Ekman transport,
66 even as far west as Herald Canyon, Pisareva et al., 2015). The final Pacific water mass found in the
67 Chukchi Sea is referred to as remnant winter water (RWW, e.g. Brugler et al., 2014). This is winter
68 water that has been warmed either by solar heating during the spring and summer or via mixing
69 with Pacific summer waters. Of all of the Pacific water masses on the northeast Chukchi shelf, the
70 NVWW has the highest nutrient content, which helps spur primary production (e.g., Lowry et al.,
71 2015). While all of the water masses pass through Barrow Canyon at some point, their seasonal
72 timing is presently unclear, as well as where geographically in the canyon they are found.

73 Ultimately the Pacific water draining through Barrow Canyon enters the interior basin, but
74 the manner by which this happens is directly influenced by the dynamics of the circulation in the
75 canyon. As depicted schematically in Fig 1, some of the Pacific water exiting the canyon turns
76 to the east and forms the Beaufort shelfbreak jet (e.g., Nikolopoulos et al., 2009). However, this
77 accounts for only a fraction of the transport through Bering Strait. Recently it has been determined
78 that a sizable portion of the Pacific water flowing out of Barrow Canyon turns to the west and forms
79 a current that progresses westward over the Chukchi continental slope. This has been named the
80 Chukchi slope current, and, using summertime data, Corlett and Pickart (2017) have determined
81 that it transports 0.5 Sv of Pacific water westward. (Unpublished data from a mooring array across
82 the continental slope to the west of Barrow Canyon has shown that the Chukchi slope current is a
83 year-round feature.) One must keep in mind, however, that the bifurcation of the flow emanating
84 from Barrow Canyon into the eastward- and westward-directed currents depicted in Fig 1 applies
85 to the mean. It is well known that the circulation in the canyon varies on short timescales. For

86 instance, the direction of the wind can strongly influence the flow, and, in particular, the behavior
 87 of the ACC (Shroyer and Pleuddemann, 2012; Okkonen et al., 2009). Eddies are also shed from
 88 the canyon (Pickart and Stossmeister, 2008), which is consistent with the vorticity structure of the
 89 canyon flow during certain times (D'Asaro, 1988; Pickart et al., 2005).

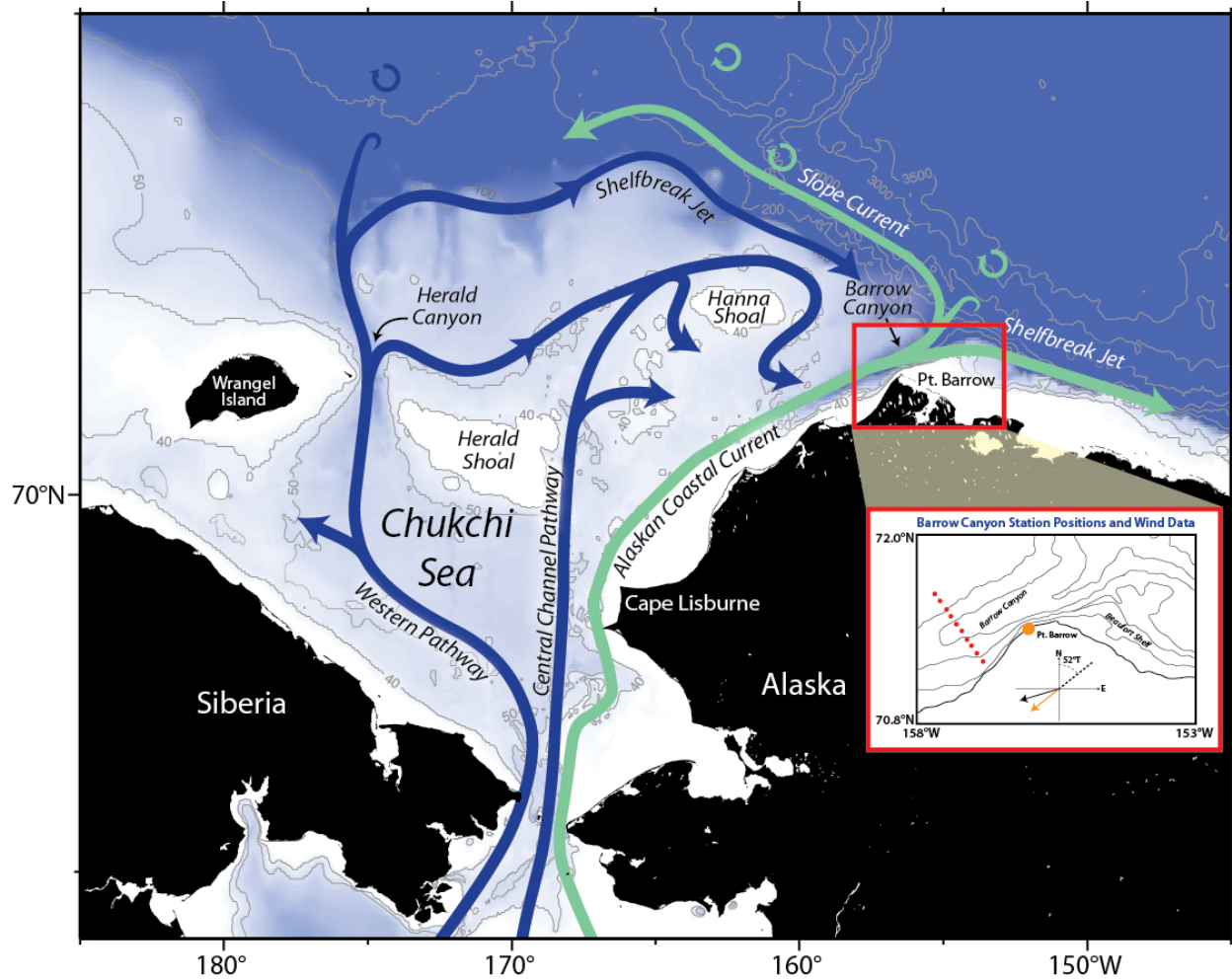


Figure 1: Map of the study area and place names. The pathways of Pacific-origin water on the Chukchi shelf, including the outflow from Barrow Canyon, is shown schematically (from Corlett and Pickart, 2017). The inset shows an enlarged view of Barrow Canyon. The nominal DBO5 station positions are shown by the red circles, and the Barrow, Alaska weather station is the orange circle. The grey arrow represents a typical 10-m wind vector, where the orange component is the along-canyon value considered in the analysis (see text).

90 Perhaps the most common mesoscale process that occurs in Barrow Canyon is upwelling. It

91 has been argued that a number of mechanisms drive such intermittent up-canyon flow. For exam-
92 ple, using mooring data Aagaard and Roach (1990) argued that eastward-propagating shelf-edge
93 waves can lead to upwelling. The modeling study of Signorini et al. (1997) suggested that time-
94 varying outflow from the shelf can result in a rectified up-canyon flow at depth. Mountain et al.
95 (1976) noted that large-scale changes in the meridional sea level gradient are a likely cause of up-
96 welling. Another obvious candidate is wind. While Aagaard and Roach (1990) found no statistical
97 correlation between the local wind and moored velocity records, there are documented instances
98 of wind-driven upwelling in the canyon (e.g., Okkonen et al., 2009; Pickart et al., 2011, Pisareva
99 et al., this issue). At times the upwelling is strong enough to advect Atlantic water (AW) well onto
100 the Chukchi shelf (Bourke and Paquette, 1976). Recently, Ladd et al. (2016) documented multiple
101 occurrences of AW as far south as Icy Cape, more than 200 km south of Barrow Canyon. Presently,
102 however, it is not known what factors dictate the ability for AW to progress into (or beyond) the
103 canyon, and what part of the canyon is in fact influenced by this warm and salty water.

104 As a choke point for Pacific water to exit the Chukchi shelf, and for Atlantic water to intermit-
105 tently flow onto the shelf, Barrow Canyon is an ideal place for studying and monitoring shelf-basin
106 exchange. As mentioned above, long-term moorings have been in place at the mouth of the canyon
107 (Itoh et al., 2013), and shorter-term mooring deployments have been carried out in the center of
108 the canyon as well as at the head (e.g., Weingartner et al., in press). While these timeseries have
109 provided a wealth of information, the spatial coverage of moorings is limited both vertically and
110 laterally. Starting in 2010, the Distributed Biological Observatory (DBO) program has facilitated
111 the occupation of a repeat hydrographic transect across Barrow Canyon. This includes physical
112 measurements as well as chemical and biological sampling. While the data collection is limited to
113 the summer months, the transects provide a high-resolution view of the hydrographic structure of
114 the canyon. This in turn offers the opportunity to assess the manner in which Pacific and Atlantic
115 water are exchanged between the Chukchi shelf and adjacent basin.

116 In this paper we use the first four years of repeat occupations of the DBO transect across Barrow
117 Canyon to investigate the distribution of water masses in the canyon and how they vary over the
118 summer and early fall. We also investigate wind-driven upwelling in the canyon and explore the

119 atmospheric circulation leading to upwelling-favorable conditions. A main goal is to provide a
120 full water column view of the hydrography of the canyon, which is impossible to obtain from
121 moorings. The outline of the paper is as follows. We begin with a description of the DBO program
122 and the shipboard hydrographic data, as well as the ancillary data used in the study. We then
123 present the mean conditions in the canyon, followed by the seasonal progression of water masses
124 from summer into fall. This is done both in the vertical plane and in temperature-salinity space.
125 Lastly, we investigate the occurrence of upwelling in the canyon and elucidate the atmospheric
126 conditions that drive this, including the patterns of storm tracks.

127 **2. Data and methods**

128 *2.1. Shipboard Hydrographic Data*

129 The primary source of data used in this study are hydrographic transects that were occupied as
130 part of the DBO program. The concept behind DBO is that, as international ships of opportunity
131 transit the Bering and Chukchi Seas doing their respective programs, they occupy one or more
132 DBO lines as time permits. Five locations have been identified as biologically active areas, or
133 "hotspots", ranging from near St. Lawrence Island in the northern Bering Sea to Barrow Canyon in
134 the northeast Chukchi Sea. Each ship participating in the program occupies a hydrographic transect
135 at one or more of the identified sites, and, to the extent practical, measures a suite of biological and
136 chemical variables – including sampling of the benthos. The objective is to construct timeseries at
137 each site that help to elucidate regional differences in the ecosystem and how this is changing as
138 the climate warms. The pilot phase of DBO began in 2010 (Grebmeier et al., 2010), and since then
139 ships from six different nations have been occupying the sites on a regular basis.

140 For the present study we use the hydrographic occupations of DBO5, the transect spanning the
141 central portion of Barrow Canyon (see the inset to Fig. 1). This section is comprised of 10 nominal
142 stations at 5 km horizontal spacing. We use the 24 occupations obtained during 2010-13, which
143 span from mid-summer to early-fall. As evidenced by the distribution of transects across years and
144 months (Table 1), there were no strong seasonal or interannual biases in the sampling.

145 Each of the cruises used a Sea-Bird Electronics 911+ conductivity-temperature-depth (CTD)

Dates	Ship	Chief Scientist
12 Jul 2010	USCGC Healy	Kevin Arrigo (Stanford University)
21 Jul 2010	CCGS Sir Wilfrid Laurier	Svein Vagle (Fisheries and Oceans Canada)
25 Jul 2010	R/V Xuelong	Jianfeng He (Polar Research Institute Of China)
24 Aug 2010	R/V Annika Marie	Carin Ashjian (Woods Hole Oceanographic Institution)
7 Sep 2010	USCGC Healy	Robert Pickart (Woods Hole Oceanographic Institution)
28 Sep 2010	R/V Mirai	Motoyo Itoh (Japan Agency for Marine-Earth Science and Technology)
20 Jul 2011	CCGS Sir Wilfrid Laurier	Svein Vagle (Fisheries and Oceans Canada)
22 Jul 2011	USCGC Healy	Kevin Arrigo (Stanford University)
29 Aug 2011	F/V Mystery Bay	Catherine Berchok (NOAA Alaska Fisheries Science Center)
1 Sept 2011	R/V Annika Marie	Carin Ashjian (Woods Hole Oceanographic Institution)
7 Oct 2011	USCGC Healy	Robert Pickart (Woods Hole Oceanographic Institution)
22 Aug 2012	USCGC Healy	Jackie Grebmeier (University of Maryland Center for Environmental Science)
24 Sept 2012	R/V Mirai	Takashi Kikuchi (Japan Agency for Marine-Earth Science and Technology)
10 Oct 2012	USCGC Healy	Robert Pickart (Woods Hole Oceanographic Institution)
21 Aug 2012	NOAAS Fairweather	Ian Hartwell (NOAA)
28 Aug 2012	F/V Aquila	Catherine Berchok (NOAA Alaska Fisheries Science Center)
23 Jul 2013	CCGS Sir Wilfrid Laurier	Svein Vagle (Fisheries and Oceans Canada)
8 Aug 2013	USCGC Healy	Lee Cooper (University of Maryland Center for Environmental Science)
14 Aug 2013	USCGC Healy	Lee Cooper (University of Maryland Center for Environmental Science)
24 Aug 2013	R/V Annika Marie	Carin Ashjian (Woods Hole Oceanographic Institution)
2 Sep 2013	R/V Aquila	Catherine Berchok (NOAA Alaska Fisheries Science Center)
3 Sep 2013	R/V Mirai	Shigeto Nishino (Japan Agency for Marine-Earth Science and Technology)
12 Oct 2013	USCGC Healy	Robert Pickart (Woods Hole Oceanographic Institution)
24 Oct 2013	USCGC Healy	Robert Pickart (Woods Hole Oceanographic Institution)

Table 1: Occupations of the DBO5 transect used in the study.

146 instrument with a SBE03 temperature sensor and SBE04 conductivity sensor. The sensors were
147 sent to Sea-Bird for pre- and post-cruise calibration. On some of the cruises the conductivity
148 sensors were also calibrated using bottle salinity data (deep water casts only). However, the DBO5
149 section is in relatively shallow water and the ranges in temperature and salinity on the Chukchi
150 shelf are quite large. As such, lack of an in-situ conductivity calibration does not impact the results
151 of our study. All of the hydrographic data were collected and processed using Sea-Bird's software,
152 ensuring consistency between the occupations. The downcast profiles were averaged into 1 db bins
153 and any small scale noise removed.

154 We constructed vertical sections of the hydrographic variables for each of the transects. The
155 variables considered were potential temperature referenced to the sea surface (hereafter referred to
156 as temperature), salinity, and potential density referenced to the sea surface (referred to as density).
157 A Laplacian-spline scheme was used to interpolate the data onto a standard grid with a vertical
158 spacing of 5 m and horizontal spacing of 2 km. The grid extends from 0 to 50 km along the x axis
159 (cross-canyon, where the positive direction is towards the Alaskan coast) and 0 to 130 m along
160 the z axis (vertical). For the temperature-salinity diagrams, the original (non-gridded) data were
161 used. The bottom topography for the standard section was constructed using soundspeed-corrected
162 echosounder data from one of the cruises.

163 *2.2. Atmospheric Reanalysis Fields*

164 In order to investigate the large-scale meteorological context during the study period, we use
165 the North American Regional Reanalysis fields (NARR, Mesinger et al., 2006). The space and time
166 resolution of NARR is 32 km and 6 hr, respectively. This product is an evolution of the original
167 National Centers for Environmental Prediction (NCEP) global reanalysis and makes use of newer
168 data assimilation and modeling advances that have been developed since then. The present study
169 uses the NARR sea level pressure data and 10 m winds. Brugler (2013) validated the NARR data
170 with the Barrow wind data described below.

171 *2.3. Meteorological timeseries*

172 For the analysis of the upwelling we use wind data from the meteorological station located in
173 Barrow, Alaska (recently renamed Utqiagvik). The data were acquired from the National Climate
174 Data Center of the National Oceanic and Atmospheric Administration (NOAA) and subject to a
175 set of quality assessment routines to remove erroneous values (see Pickart et al., 2013, for details).

176 *2.4. Ice concentration data*

177 For the ice concentration analysis, we used the Ice Coverage Percentage as derived from a
178 combination of the following two passive Microwave satellite sensors: the Advanced Very High
179 Resolution Radiometer (AVHRR) and the Advanced Microwave Scanning Radiometer - Earth Ob-
180 serving System (AMSR-E), both of which have been objectively interpolated onto a daily grid.
181 The spatial resolution of the blended product is 0.25 degrees.

182 **3. Results and Discussion**

183 *3.1. Water Mass Analysis*

184 *3.1.1. Mean State*

185 Using all 24 DBO5 occupations we created mean vertical sections of temperature, salinity,
186 and density for the July-October period when the ship occupations occurred (Fig. 2). Using the
187 AMSR-E data we documented the ice concentration in the study region for each of the occupations.
188 According to the AMSR-E ice concentration product, in every case there was open water in Barrow
189 Canyon and in the surrounding area as well. The ice edge was typically far to the north of the
190 transect.

191 To our knowledge, Fig. 2 represents the first mean view across Barrow Canyon that encom-
192 passes the entire water column. The warmest water in the section ($> 4^{\circ}\text{C}$) is found above the
193 eastern-most part of the canyon, which is due to the presence of ACW. The temperature front cor-
194 responding to the ACW is located near $x=33$ km, where the 4°C temperature contour outcrops
195 and the 2°C contour descends abruptly to deeper depths. Notably, there is a density front here as
196 well where the isopycnals start to slope downward progressing onshore. This is consistent with a

197 surface-intensified ACC advecting this warm water out of the canyon; farther to the east the Beau-
 198 fort shelfbreak jet is surface intensified when it transports ACW at this time of year (von Appen
 199 and Pickart, 2012). This thermal wind signature in the canyon indicates that the ACC extends to
 200 > 100 m and transports more than just ACW. The mean salinity section reveals that the ACW is
 201 not the freshest water found in the canyon. There is a layer of low-saline meltwater/runoff in the
 202 upper 20 m of the water column on the western side of the canyon (discussed further below).

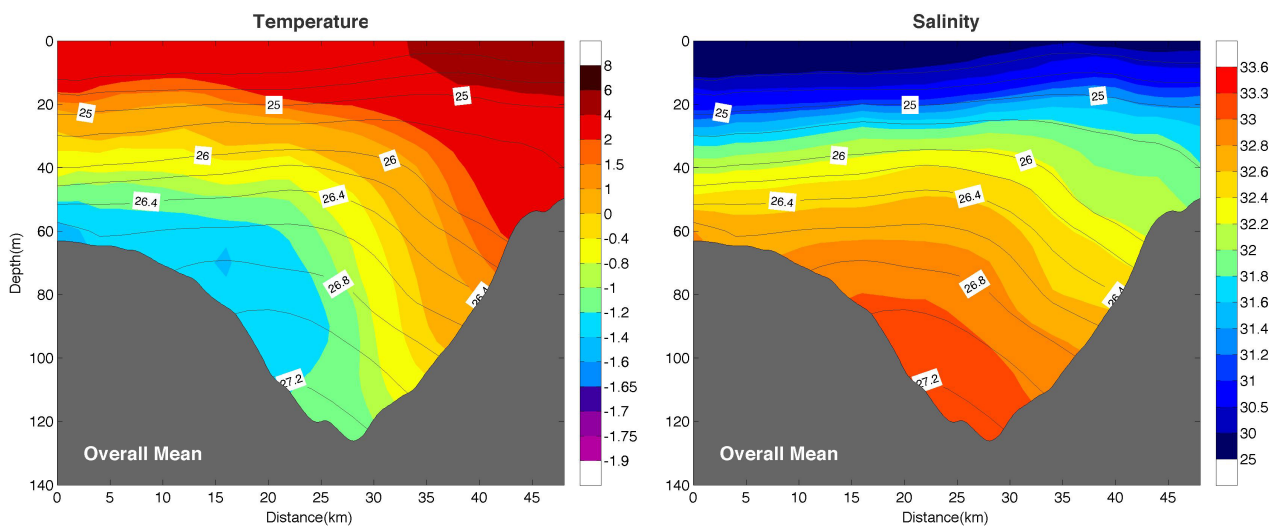


Figure 2: Mean vertical sections of hydrographic properties from the 24 occupations of the DBO5 line. (a) Potential temperature ($^{\circ}\text{C}$, color) overlain by potential density (kg m^{-3} , contours). The viewer is looking to the north. (b) Same as (a) except for salinity (color).

203 The coldest water in Barrow Canyon at this time of year is banked against the western side of
 204 the canyon, extending onto the interior shelf. It is perhaps surprising that this cold winter water
 205 is not found at the deepest part of the canyon, but this is likely due to a combination of factors.
 206 In their analysis of a synoptic survey of the canyon, Pickart et al. (2005) determined that NVWW
 207 sinks as it flows down the canyon; however, the canyon deepens rapidly to the north and the dense
 208 water finds an equilibrium depth well above the bottom due to the stratification. Another thing to
 209 note is that the densest winter water on the Chukchi shelf is not always the coldest. Finally, warm
 210 AW was present at the bottom of the canyon in some of the occupations (see the upwelling analysis
 211 in Section 3.2). Although we do not have velocity information, we can infer that, in the mean, the

212 winter water is being fluxed northward as a bottom-intensified flow. This is consistent with the fact
213 that the isopycnals slope upward from the western side of the canyon towards the center (down to
214 a depth of about 50 m). Our mean sections thus reveal that, during the summer months, ACW is
215 advected northward on the eastern side of the canyon while winter water is transported northward
216 on its western flank. We note that, farther to the north, some of the winter water transposes to the
217 other side of the canyon (Pickart et al., 2005) and enters the Beaufort shelfbreak jet, while some of
218 it remains on the western side and feeds the Chukchi slope current (Corlett and Pickart, 2017).

219 It is impossible to identify in the mean vertical sections precisely where all of the different water
220 masses are situated, simply because, in the process of constructing the mean, they are averaged
221 together to a certain degree. Hence, to investigate the presence of the various water types we
222 computed a volumetric temperature-salinity (T/S) diagram (Fig. 3). In particular, we divided the
223 T/S domain into bins and tabulated the number of realizations within each bin. The water mass
224 boundaries in Fig. 3 are the same as those used in previous studies (e.g., Lin et al., 2016; Corlett
225 and Pickart, 2017). We note, however, that these boundaries are not precise; for instance, there is
226 interannual variability of the water properties flowing through Bering Strait (e.g., Pisareva et al.,
227 2015). Nonetheless, the basic definitions used here are robust. As mentioned above, we consider
228 four Pacific water masses: NVWW, RWW, BSW, and ACW, as well as AW and meltwater/runoff
229 (MW).¹

230 It is clear that winter water (i.e. NVWW and RWW) is the most common water type found
231 in Barrow Canyon during the summer and early-fall (Fig. 3). Most of this falls within a narrow
232 T/S range. NVWW has a very high nutrient concentration (e.g. Pickart et al., 2016), which is
233 known to promote phytoplankton growth on the Chukchi shelf and in Barrow Canyon (e.g. Hill
234 et al., 2005; Lowry et al., 2015). The next most common water mass is BSW. As noted in the
235 introduction, this is believed to be primarily a mixture between Anadyr water and central Bering
236 shelf water. However, as demonstrated by Gong and Pickart (2016), the densest and most weakly
237 stratified type of BSW is in fact a modification of RWW. In particular, in early summer the RWW

¹BSW has also been called western Chukchi summer water (Shimada et al., 2001) and Chukchi summer water (von Appen and Pickart, 2012).

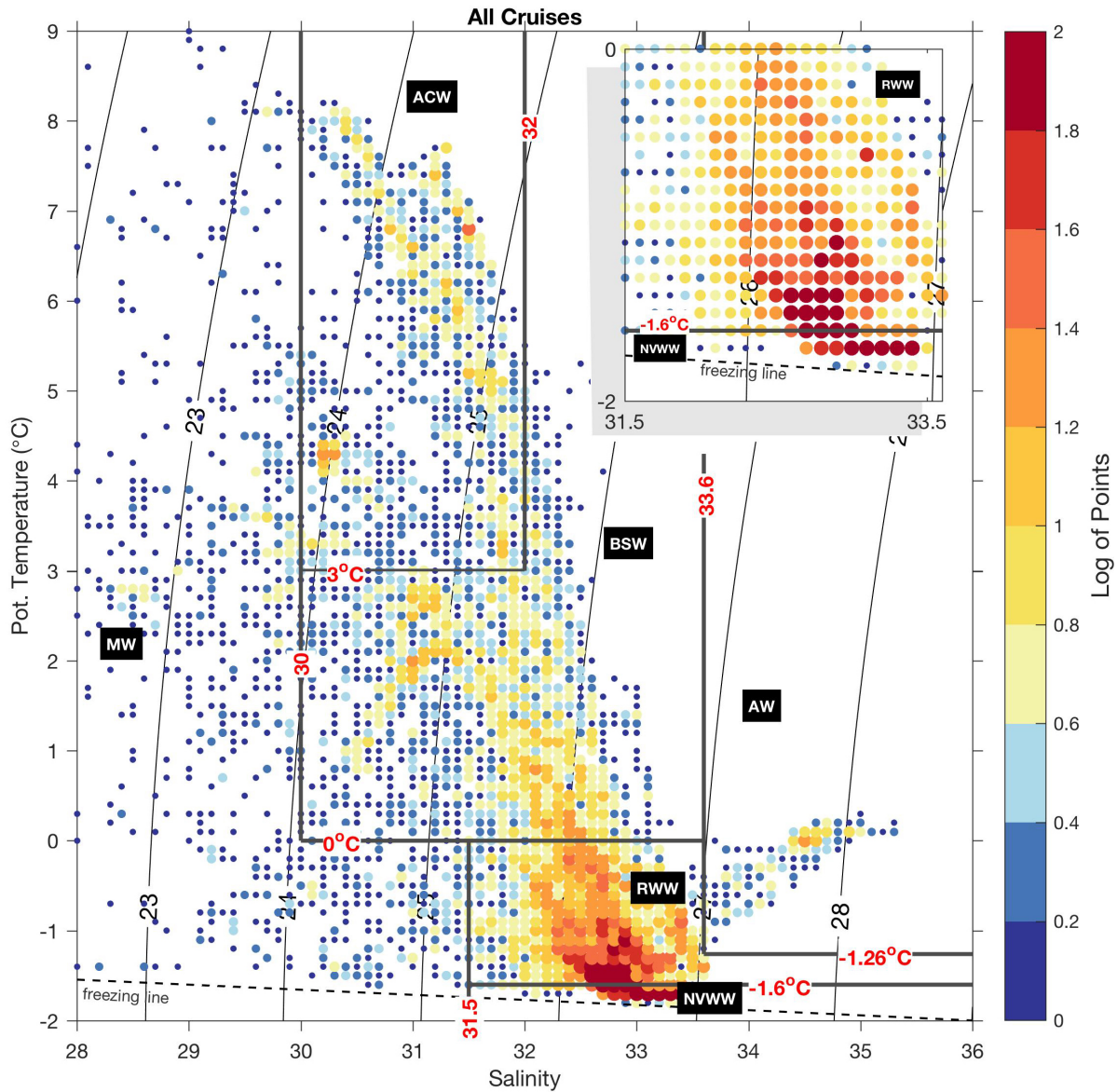


Figure 3: Temperature-salinity diagram for all of the DBO5 occupations. The color corresponds to the frequency of occurrence of water within bins of 0.1°C in temperature by 0.1 in salinity. The water mass boundaries are indicated by the grey lines. The inset shows an enlarged view of the winter water. The different water masses are: NWWW = newly ventilated winter water; RWW = remnant winter water; BSW = Bering summer water; ACW = Alaskan coastal water; MW = meltwater/runoff; and AW = Atlantic water.

238 can be warmed either by solar heating within polynyas or by mixing with ACW along the ACC
239 pathway, which converts the properties of the water to that of BSW. This is likely the reason for
240 the large amount of BSW colder than 1°C in Fig. 3. Note that there is another (smaller) peak in
241 BSW between 2-3°C that is fresher; the nature of this signal is explained in the next section.

242 While ACW is found in many of the DBO5 occupations, its relative presence is much smaller
243 than the other Pacific water masses. There are two “branches” of ACW in T/S space: a warmer,
244 saltier branch and a colder/fresher branch. This is a seasonal effect which is discussed below.
245 The two non-Pacific water masses found in the canyon are MW and AW. As seen in the mean
246 vertical section of salinity, the former resides in the near-surface layer, while the latter appears
247 intermittently near the base of the canyon (not evident in the mean vertical sections).

248 *3.1.2. Seasonality*

249 *Temperature-salinity space*

250 There are clear trends in the water masses flowing through Barrow Canyon as the season pro-
251 gresses from July to October. This is demonstrated by constructing monthly versions of the volu-
252 metric T/S diagrams, which are shown in Fig. 4. Considering the winter water first, one sees that
253 NVWW is only present in appreciable amounts during the month of August (see the insets). It is
254 not immediately clear why this time range is so narrow. NVWW flows northward through Bering
255 Strait through much of the winter and spring. Typically, the water in the strait is at or near the
256 freezing point from January through April (Woodgate et al., 2005). Some of this NVWW water
257 progresses into Barrow Canyon via the swift coastal pathway; data from the canyon indicate that
258 it is present there in May and early-June (Codispoti et al., 2005; Weingartner et al., 2013; Pickart
259 et al., 2016). However, the DBO data presented here, as well as other hydrographic data collected
260 in June and July in the canyon (Gong and Pickart, 2015; Pickart et al., 2016), suggest that the last
261 of the NVWW in the coastal jet has passed through the canyon before the end of June.

262 This begs the question, what is the source of NVWW present in Barrow Canyon in August and
263 what dictates this timing? This is partially answered by considering the results of Pickart et al.
264 (2016) who analyzed an extensive hydrographic/velocity survey of the northeast Chukchi shelf
265 in June-July 2011. They determined that the Central Channel pathway (with a contribution from

266 the western pathway) bifurcates as it encounters Hanna Shoal, and, at this time of year, NVWW
267 flows around both sides of the shoal towards Barrow Canyon. This is depicted schematically in
268 Fig. 1 (for a detailed circulation map, see Figure 9 of Pickart et al., 2016). It is also seen in the
269 numerical model of Shroyer and Pickart (this issue). In the 2011 shipboard survey of the shelf, the
270 leading edge of the NVWW (which originated from Bering Strait) was located on the eastern side
271 of Hanna Shoal in the middle of July, while the trailing edge was north of the Central Channel still
272 a fair distance away from the shoal at the beginning of July. The average speed of the winter water
273 was 10 km/d, and, based on the circulation diagram in Pickart et al. (2016), the distance from the
274 leading edge to the center of Barrow Canyon (see the schematic of Fig. 1) is 300 km. This implies
275 that the arrival time of the NVWW at the DBO5 line should be mid-August, which is consistent
276 with the data presented here. Using similar reasoning, the trailing edge of the NVWW should pass
277 through the canyon at the end of August / early September, again in line with our observations.
278 Hence, it appears that the central shelf pathways deliver a second pulse of NVWW into Barrow
279 Canyon during the August time frame.

280 Fig. 4 indicates that RWW is present in Barrow Canyon during each of the months, although
281 it is found in greatest amounts in August and September. This makes sense in light of the above
282 results. Recall that RWW is simply NVWW that has been warmed by solar heating and/or mixing
283 with summer waters. September has the largest amounts of the densest variety of RWW, which is
284 likely due to the moderation of some of the NVWW pulse circulating around Hanna Shoal.

285 BSW is also present during each of the months, but there are seasonal differences. In particular,
286 there are large amounts of relatively dense BSW in July and August, which in part may be due to
287 conversion of RWW to this water mass as noted above (and described in detail in Gong and Pickart,
288 2016). Note, however, that in October a separate peak of warmer and fresher BSW appears. This
289 could be the result of cooling of ACW. One sees that the presence of the warm ACW is greatest in
290 August and September, in line with the seasonal development of runoff and the ACC. In early fall,
291 cold air and enhanced winds cool the ACW; indeed, the ACW signature has “collapsed” to colder
292 temperatures in October (Fig. 4). Continued cooling would then transform this into the warm,
293 fresh variety of BSW observed in October. Therefore, based on our data, it can be deduced that a

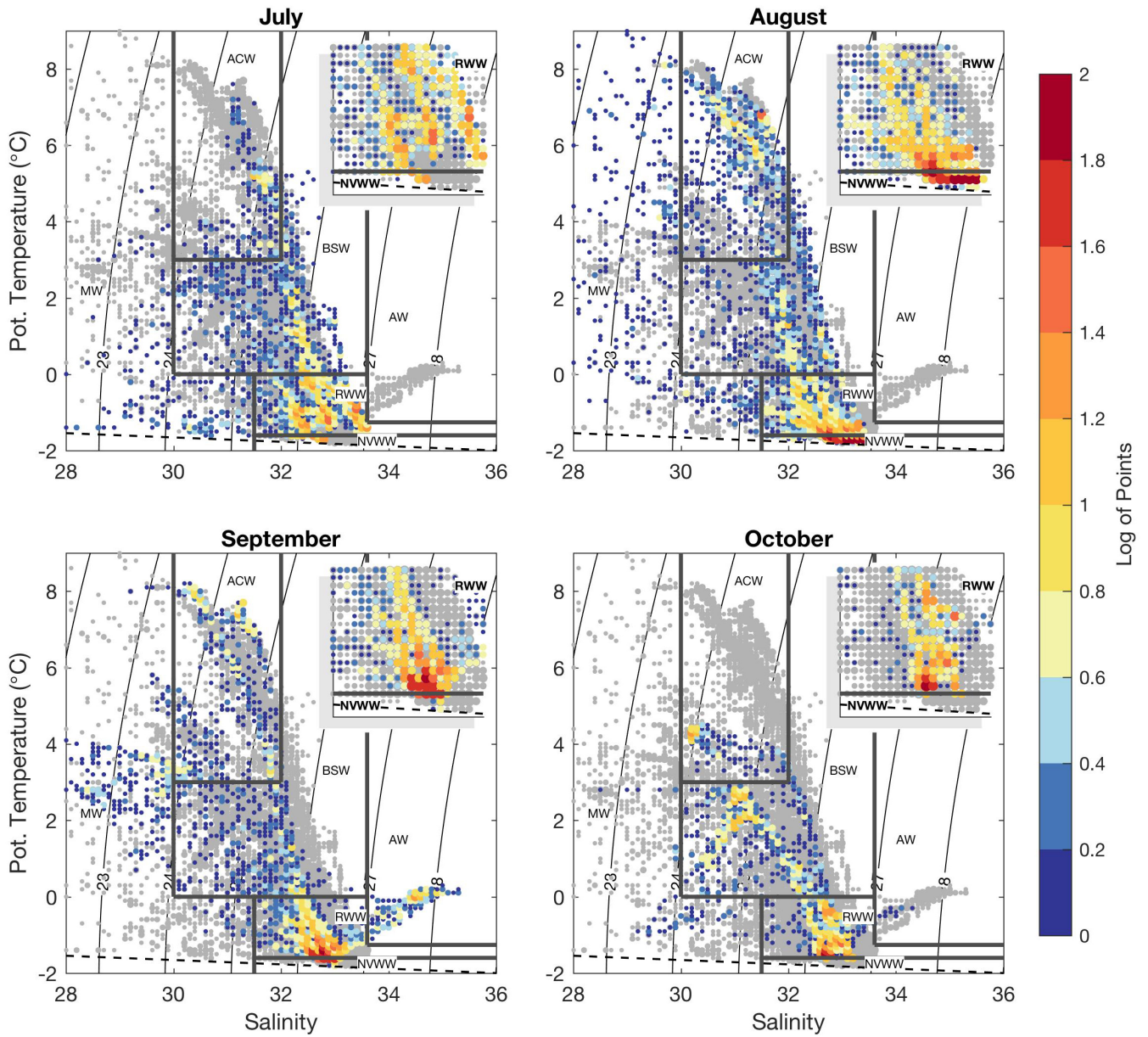


Figure 4: Temperature-salinity diagrams for the months of (a) July, (b) August, (c) September, and (d) October. The color represents the frequency of occurrence as in Fig. 3. The insets show enlarged views of the winter water. The grey dots denote the data from all of the occupations. See the caption to Fig. 3 for the water mass names.

294 significant amount of the BSW that flows through Barrow Canyon on its way to the interior basin
295 is formed by local processes on the shelf. This is in contrast to the notion that this water mass is
296 mainly a mixture of Anadyr water and Bering shelf water entering Bering Strait.

297 The character of the MW evolves from summer into fall as well. In July and August there are
298 relatively large amounts of cold, salty water – i.e. early-season MW that is presumably influenced
299 by mixing with winter water. In August into September, however, much warmer MW is present in
300 the occupations. This is likely due to solar heating and a larger contribution from runoff (Cooper
301 et al., 2016; Gonsior et al., 2017). Then in October the MW signature diminishes substantially,
302 probably the result of mixing (the same process that modifies the ACW that month). Finally, our
303 seasonal T/S plots reveal that most of the AW observed in Barrow Canyon was present during the
304 month of September (none at all in July and August). This is addressed below in section 3.2.

305 *Geographical space*

306 We now investigate the seasonal presence of the different water masses in the vertical plane,
307 which offers insights regarding the circulation in the canyon and the ultimate fate of the water.
308 Using the water mass definitions in Fig. 3, we went through all of the synoptic occupations and
309 determined where in the section each water type was located. This was then tabulated for each
310 month as follows. For a given occupation, if a particular water mass was present, we shaded this
311 part of the section a semi-transparent grey. These plots were then overlaid for each of the four
312 months (Figs. 5–10). Hence, the darker the grey tone, the more realizations of that water mass
313 during the month in question.

314 Consider first the ACW (Fig. 5). One sees that this water mass is generally found on the eastern
315 side of the canyon above 60 m depth (consistent with the mean section of Fig. 2). Seasonally, it
316 is more confined geographically (closest to the coast and shallowest) in July. It is most prevalent
317 in August where there is a well-defined "wedge" inshore of $x=35$ km. Then in September more
318 ACW is found offshore, extending to the western end of the section; this is because of the upwelling
319 favorable winds that month (see section 3.2 below). Finally, in October only one of the transects
320 measured ACW. The other warm Pacific water mass, BSW, shows less variation through the course
321 of the four months (Fig. 6). As is the case with the ACW, this water mass is most prevalent on the

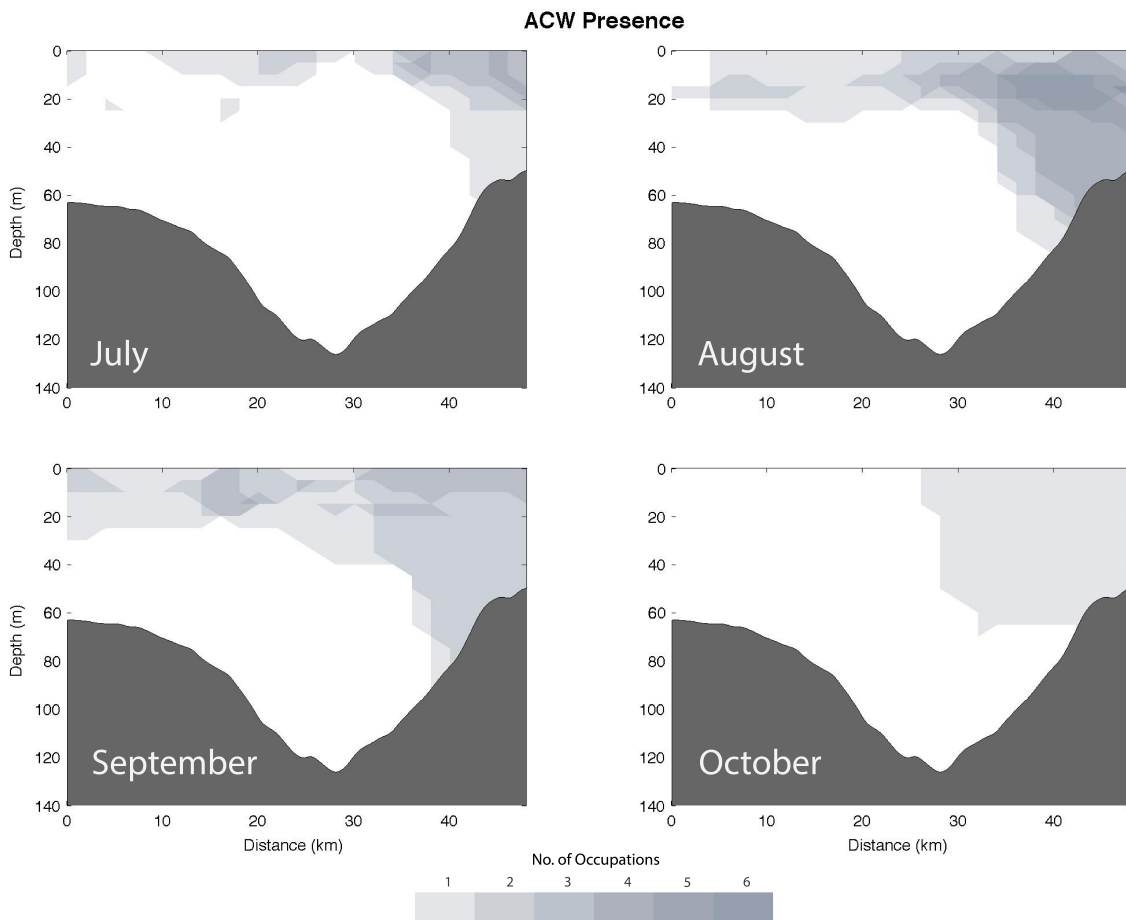


Figure 5: Monthly presence of ACW. Grey shading marks where this water mass is present in each realization within the given month. The colorbar indicates the number of realizations.

322 eastern side of the canyon and sometimes occupies the same location in the water column as the
 323 ACW. It does, however, extend a bit deeper. Our data suggest that BSW flows out of the canyon
 324 more steadily than the ACW.

325 As noted above, NVWW mainly appears in the Canyon during the month of August. The ver-
 326 tical sections indicate that only a tiny amount of this water type is present in the other months (and
 327 none at all in October, Fig. 7). As was evident in the mean section, this water mass flows north-
 328 ward mainly banked against the western flank of the canyon. However there is synoptic variability
 329 in the position of the core, and at times it is found on the western edge of the canyon, while at

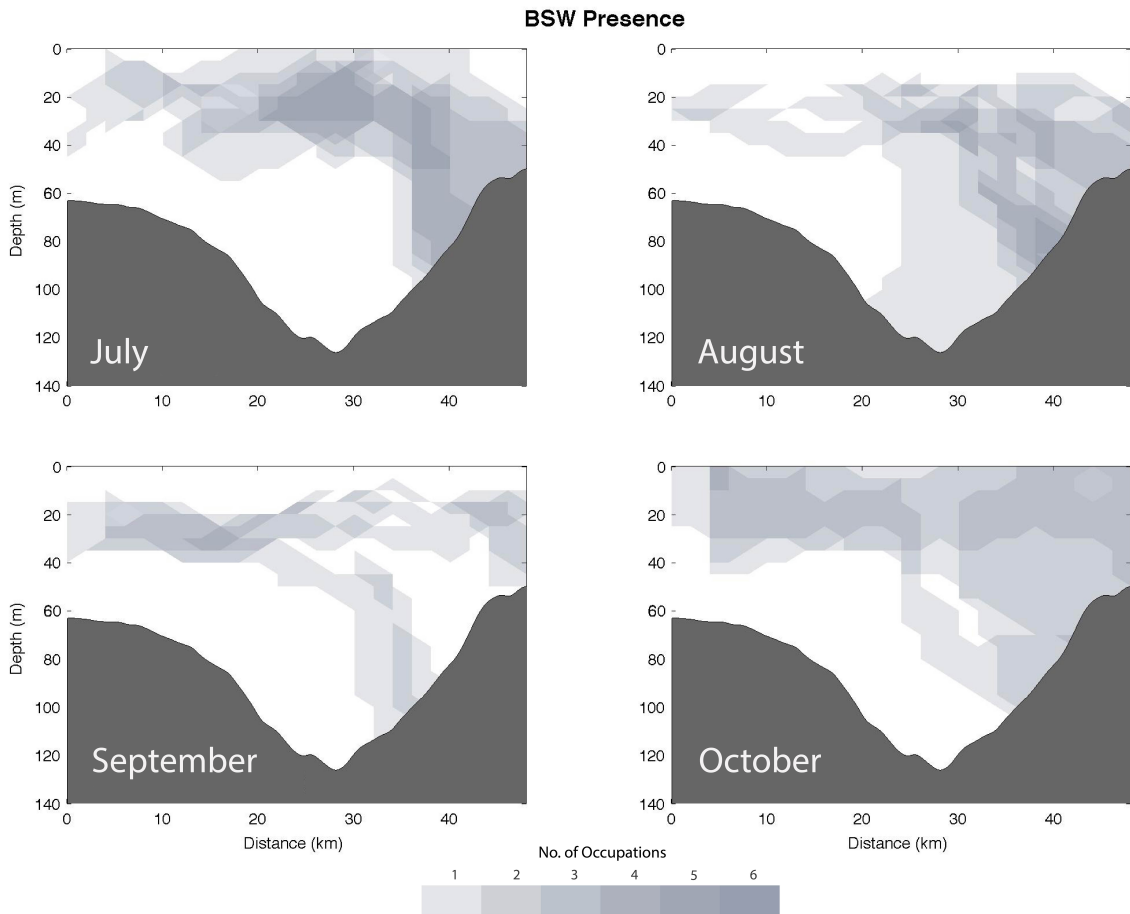


Figure 6: Same as Fig. 5 except for BSW.

330 other times it extends onto the base of the eastern flank. As explained above, the source of the
 331 NVWW in Barrow Canyon at this time of year is the central shelf. Based on a mass budget of
 332 the northeast Chukchi Sea, Pickart et al. (2016) deduced that the water flowing anti-cyclonically
 333 around the northern side of Hanna Shoal feeds the western side of Barrow Canyon. This is con-
 334 sistent with presence of NVWW observed in Fig. 7. By contrast, RWW is found in large amounts
 335 on both sides of the canyon (Fig. 8), although it is present more often on the western flank. There
 336 was a significant amount of RWW observed in each month, although a lesser quantity was found
 337 in October. Note that in August the RWW was more confined to the middle of the water column,
 338 in particular at the edges of the NVWW.

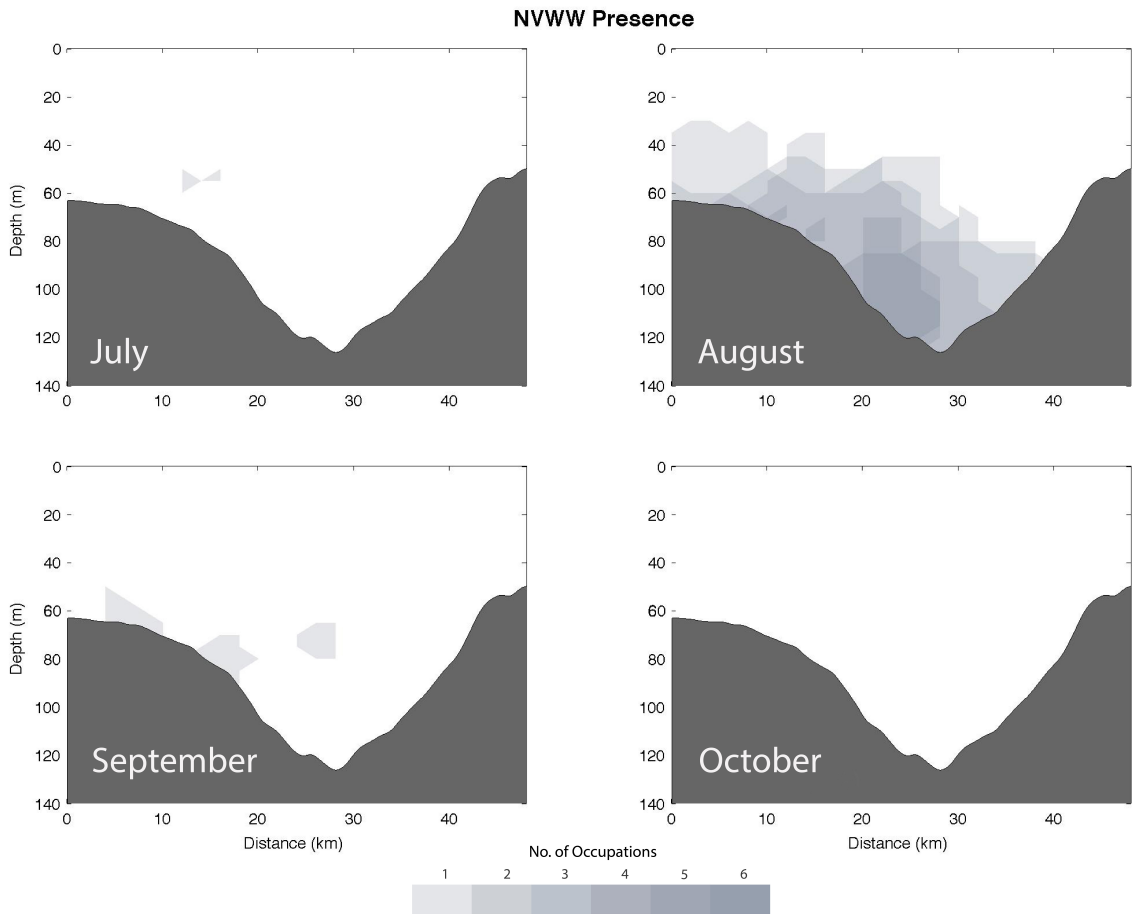


Figure 7: Same as Fig. 5 except for NVWW.

339 Early in the season (July and August), the majority of the MW is found on the offshore side of
 340 the canyon in the top 20 m (Fig. 9), although there is a small amount present in the ACC in August.
 341 Recall that during these months the MW is colder and saltier (see Fig. 4). It makes sense then that
 342 more of it is found offshore because the ACW tends to melt the ice in the ACC pathway earlier
 343 than this (Weingartner et al., 1998). In the latter two months, the warmer variety of MW (i.e. with
 344 an increased contribution due to runoff) is more evenly distributed across the canyon. Lastly, the
 345 AW is found near the bottom all along the eastern flank of the canyon (Fig. 10). As noted above it
 346 was observed predominantly in September, with a small amount present in October. This signature
 347 of AW arises because of wind-driven upwelling, which is described next.

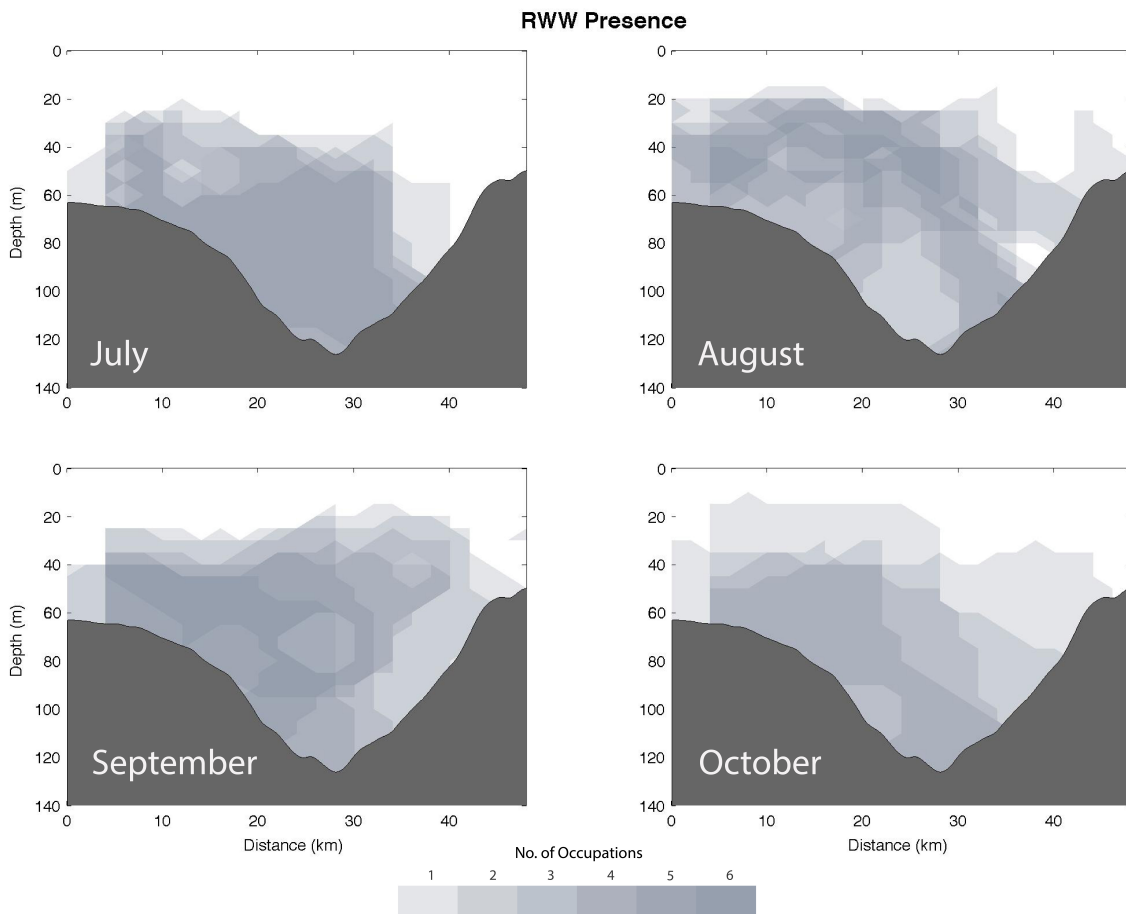


Figure 8: Same as Fig. 5 except for RWW.

348 3.2. Upwelling

349 As discussed in the introduction, upwelling occurs fairly regularly in Barrow Canyon, often
 350 driven by winds. We now consider those sections that were occupied under enhanced northeast-
 351 erly winds in order to elucidate the hydrographic response within the canyon to such upwelling-
 352 favorable conditions.

353 First it was necessary to characterize the winds in an objective manner. During an upwelling
 354 event, denser water from the basin is advected up the canyon, appearing near the deepest part of
 355 the DBO5 line and also along the eastern flank of the canyon. As such, we computed the average
 356 density anomaly over this region for each of the 24 occupations and compared this to the Barrow

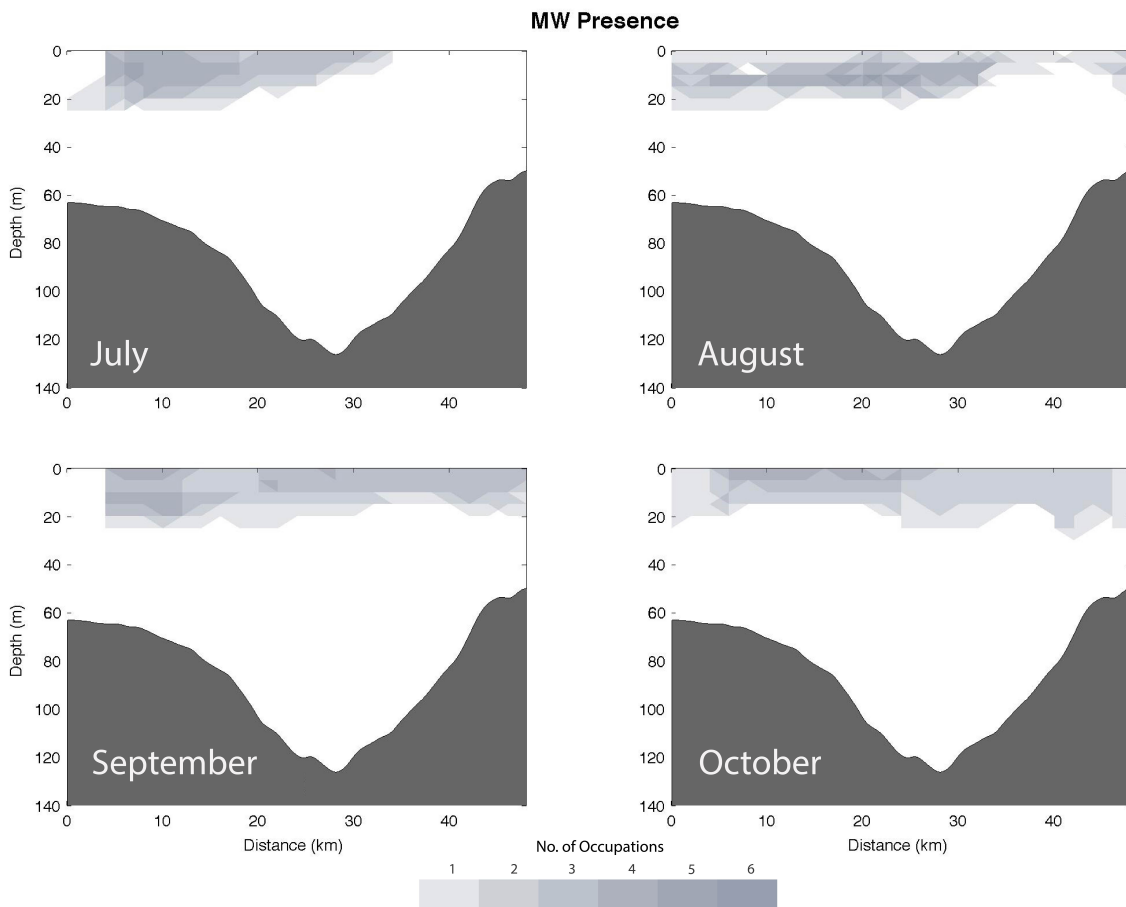


Figure 9: Same as Fig. 5 except for MW.

357 wind record. The highest correlation between the density anomaly and the wind record was for
 358 the component of wind along 52°T , which is approximately the axis of the canyon. This is not
 359 surprising, and is in agreement with the findings of Pisareva et al. (this issue) who deduced the
 360 same angle using two years of wind and mooring data from the early 2000s. Empirically, the
 361 clearest relationship between the wind and density anomaly occurred when we considered the
 362 wind over a three-day window prior to the mid-point time of the section. Those sections when the
 363 along-canyon wind speed exceeded 6.5 m/s for 20 hrs within this window were deemed upwelling
 364 realizations. We note that, while these are the optimal parameters, our results are not sensitive to
 365 the precise values.

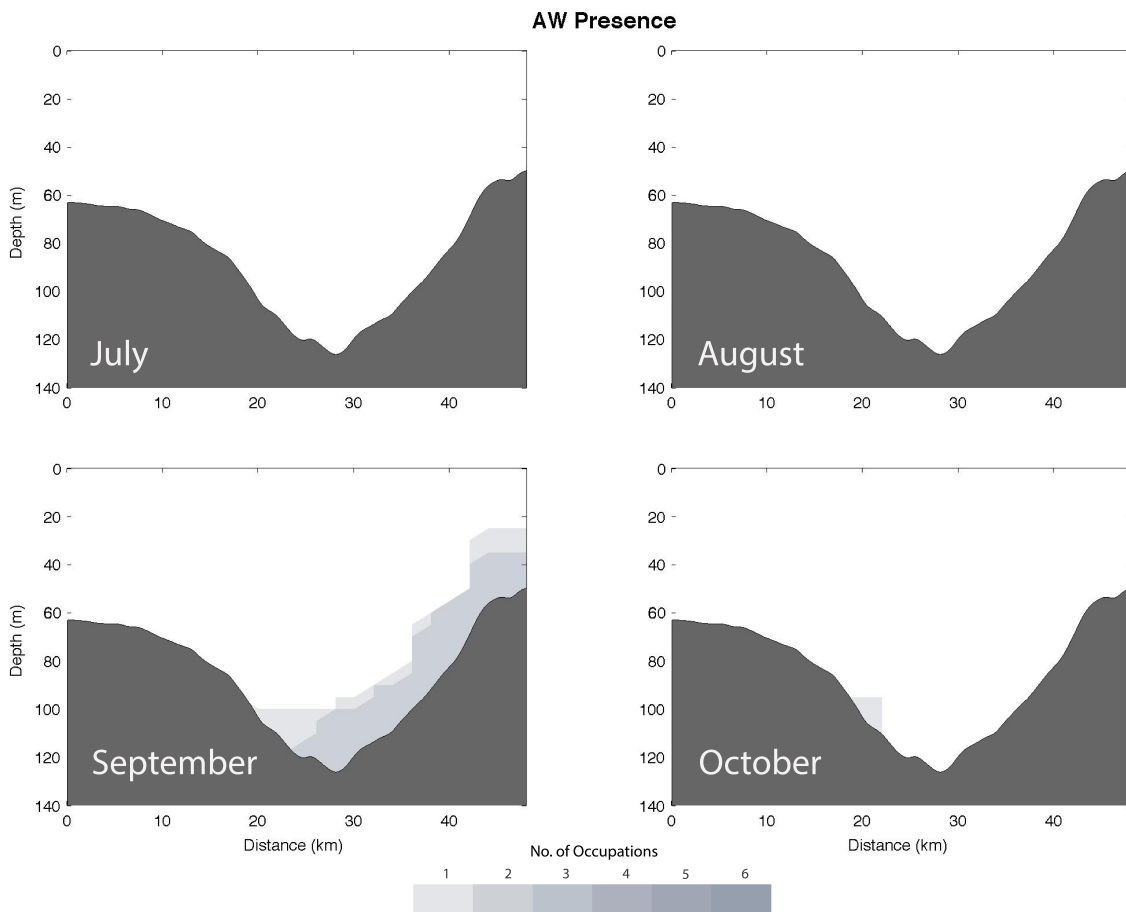


Figure 10: Same as Fig. 5 except for AW.

366 Based on the above criteria, 7 of the 24 sections were occupied during upwelling favorable
 367 conditions (Table 2): two in July, one in August, two in September, and two in October. In three
 368 cases AW was observed in the section (the only three such occupations out of the 24). The other
 369 upwelling realizations contained Pacific water at the base of the canyon (see Table 2). It should
 370 not come as a surprise that upwelling was observed in each of the months and that not all of the
 371 cases involved AW. Using two years of mooring data on the Beaufort slope (roughly 150 km to the
 372 east of Barrow Canyon), Schulze and Pickart (2012) found that upwelling occurred throughout the
 373 year and that in only 25% of the cases was AW advected onto the shelf.

374 Notably, there was no obvious correlation between different wind metrics and the type of water

Date of section	Upwelled water mass	Peak wind speed (m/s)	Mean wind speed (m/s) ($\overline{u_w}$)	Strong wind hours (t_w)	$C_{EK} = \overline{u_w} \times t_w$
12 Jul 2010	RWW	11.9	7.6	22	167
21 Jul 2010	RWW	10.5	8.5	34	290
7 Oct 2011	RWW	9.4	7.6	28	213
24 Sep 2012	AW	10.2	8.2	11	90
3 Sep 2013	AW	14.2	11.4	27	307
8 Aug 2013	NVWW	11.8	8.3	22	182
12 Oct 2013	AW	12.2	9.1	15	136

Table 2: Upwelling metrics for the transects occupied under enhanced up-canyon winds.

375 upwelled (Table 2). This was the case when considering the peak wind speed over the time period
376 that the wind exceeded 6.5 m/s, the mean wind speed over this period, the number of hours of
377 strong winds, and the product of the latter two quantities defined as C_{EK} (taken as a measure of
378 the cumulative Ekman transport, Huyer et al., 1979; Pisareva et al., 2015). One might expect that
379 AW would be advected into the canyon only during strong storms. However, Table 2 shows that
380 AW was upwelled during storms with both large and small values of C_{EK} . Furthermore, RWW
381 was upwelled for the storm with the second largest value of C_{EK} . One of the factors at play here
382 is the type of water that resides offshore of the canyon at the onset of a given storm, which varies
383 seasonally. As noted above, NVWW exits the canyon during the month of August (Fig. 7), and
384 this water was found in the canyon during the August upwelling event (Table 2). Interestingly, in
385 this realization the cold dense water was found on the eastern flank of the canyon, as opposed to
386 the more typical scenario of residing on the western flank. The reader is directed to Pisareva et al.
387 (this issue) for a more thorough investigation of the type of water upwelled in Barrow Canyon over
388 the course of the full year.

389 In order to characterize the hydrographic structure of the canyon during upwelling, we com-
390 posited the 7 upwelling transects and compared this to the composite of the 17 non wind-forced
391 realizations (Fig. 11). The mean unforced state shows the same basic features of the overall mean:
392 the ACW resides above the eastern edge of the canyon while the winter water is banked on the
393 western flank (compare Fig. 2 and Fig. 11a,b). However, the upwelled state is markedly dif-

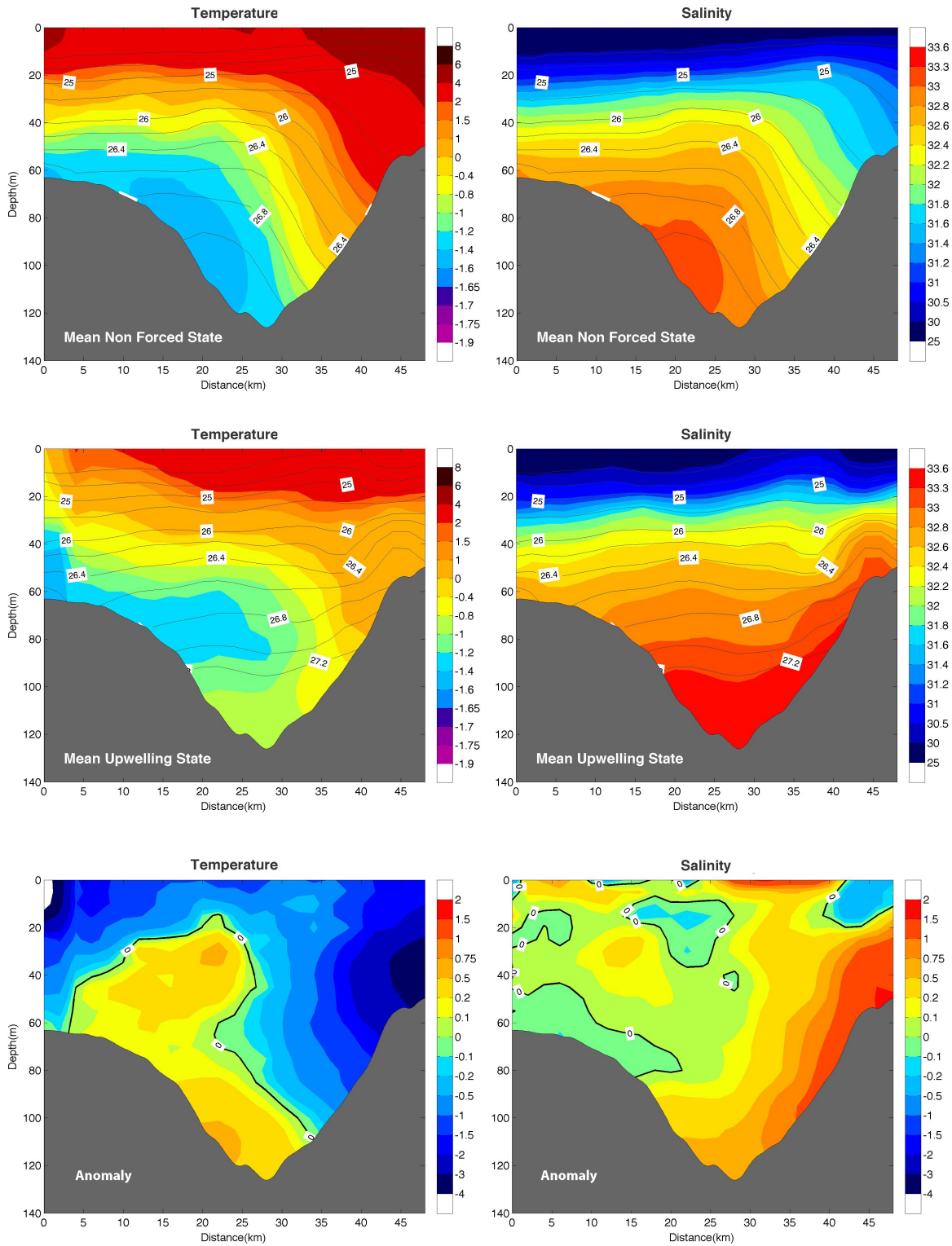


Figure 11: Composite vertical sections of the upwelling realizations compared to the non wind-forced realizations. Top panel: non-forced mean. (a) potential temperature ($^{\circ}\text{C}$, color) overlain by potential density (kg m^{-3} , contours); (b) salinity (color) overlain by potential density (contours). Middle panel: upwelling mean. (c) potential temperature (color) overlain by potential density (contours); (d) salinity (color) overlain by potential density (contours). Bottom panel: anomaly sections (upwelling minus non-forced). (e) potential temperature ($^{\circ}\text{C}$); (f) salinity. The thick black line marks the zero contour.

394 ferent. The composite reveals that warmer, saltier water is present at the bottom of the canyon
395 (Fig. 11c,d). While this salinity signal extends up the eastern flank, the same is not true for the
396 temperature. This is made more clear by considering the anomaly sections (Fig. 11e,f). One sees
397 that the salinity anomaly extends onto the eastern shelf and is in fact strongest at this shallow lo-
398 cation. By contrast, while the temperatures are warmer at the bottom of the canyon, they become
399 distinctly colder progressing up the eastern side of the canyon. As is true for salinity, the largest
400 temperature anomaly is on the shelf. The likely explanation for this is that the Pacific winter water
401 layer (be it NVWW or RWW) is advected up the canyon wall, displacing the BSW and ACW that
402 normally reside there at this time of year (see Section 3.1.2), while the AW more readily influences
403 the bottom of the canyon.

404 Another interesting hydrographic feature associated with the upwelling is the cooling of the
405 surface layer across the entire transect, which is particularly evident in the temperature anomaly
406 section (Fig. 11e). The reasons behind this are less clear. While Ekman transport should advect
407 warm ACW offshore, wind mixing would tend to cool these waters. The hydrographic response
408 of the surface layer also depends on the state of the ACC. Okkonen et al. (2009) found that, for
409 northeasterly winds, the ACC is displaced offshore. However, for strong enough winds the current
410 could possibly reverse to the south (although the storms considered here were not particularly
411 powerful, Table 2). Clearly there are different factors at play, and the near-surface cooling observed
412 here, as well as the cooling of the entire water column on the western edge of the canyon, merits
413 further investigation (perhaps in a numerical framework).

414 Finally, it is worth documenting the upwelling response in T/S space (Fig. 12). While it is not
415 meaningful to compare the frequency of water mass occurrences between the upwelling and non-
416 forced states (there are far more non-forced realizations), the patterns show some clear differences.
417 Most notably, the only time that AW was present in Barrow Canyon at the DBO5 transect was
418 during wind-driven upwelling events. Conversely, the only time that ACW was present at this site
419 was during periods of relatively weak winds. It was noted earlier that, in October, a warmer variety
420 of BSW appears at the DBO5 line which we argued was due to the conversion of ACW to BSW
421 via atmospheric cooling. Fig. 12 reveals that this occurred during upwelling events. This suggests

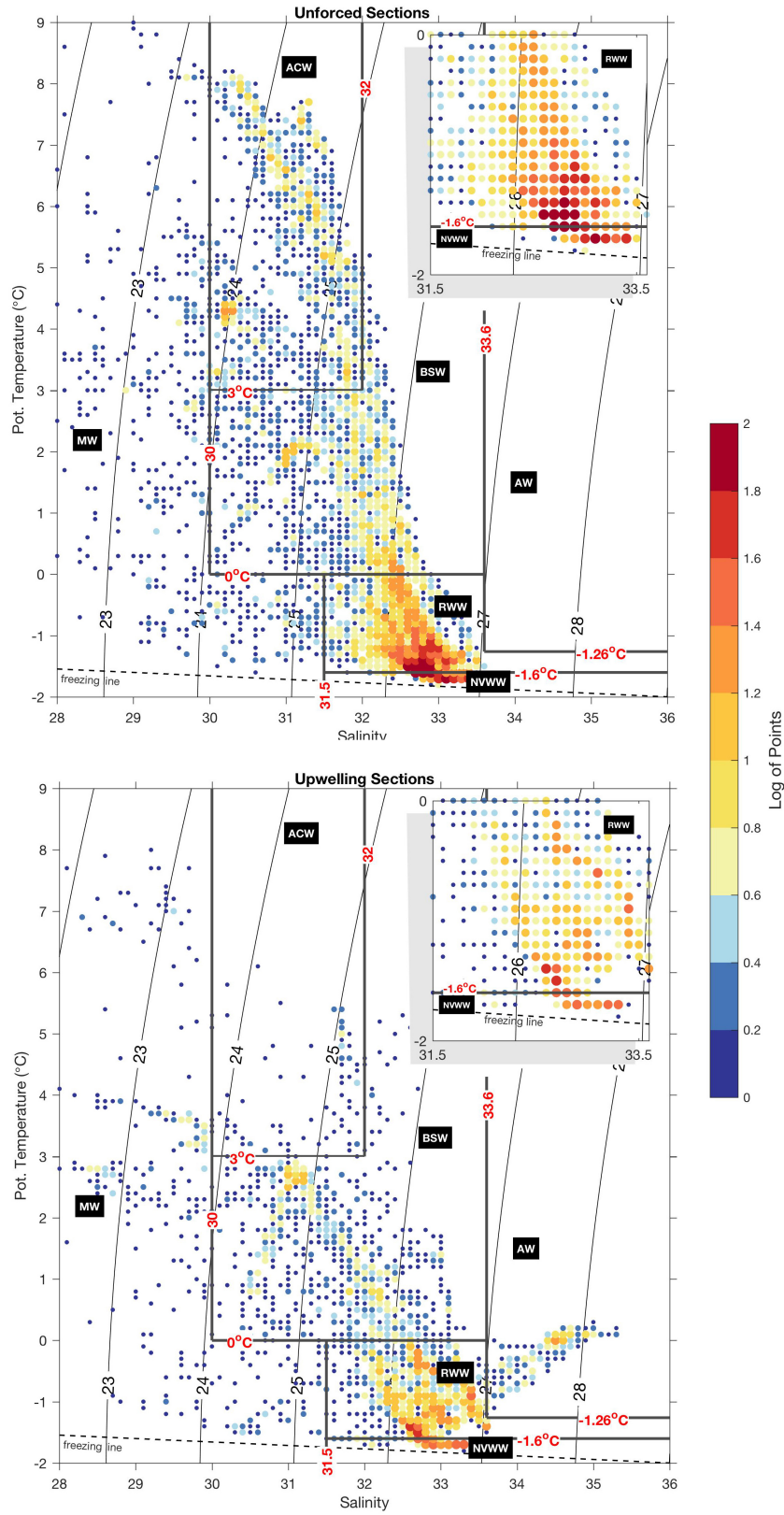


Figure 12: Temperature-salinity diagrams for the (a) non wind-forced DBO5 transects and (b) upwelling transects. The color represents the frequency of occurrence as in Fig. 3. The insets show enlarged views of the winter water distribution.

422 that wind-induced mixing can play an important role in the conversion of one Pacific water mass
423 to another.

424 *3.3. Atmospheric Forcing*

425 To examine the atmospheric conditions associated with upwelling, we used the Barrow wind
426 data to identify all of the events that likely occurred during the months of July–October during
427 2010–2013 (i.e. not just the 7 cases when shipboard data were being collected in the canyon). In
428 particular, we found all of the periods during which the up-canyon wind speed exceeded 6.5 m/s,
429 where the length of the event was taken to be the time when the winds were stronger than the
430 e-folding value of the peak wind (discounting any short dips below this threshold). Only events
431 that were longer than 20 hours were considered. Over the four-year study period there were 95
432 events totaling 178 days (versus 311 days of non-upwelling conditions).

433 Previous studies (e.g., Itoh et al., 2013; Pickart et al., 2013; Brugler et al., 2014) have demon-
434 strated that the wind measured at Barrow is largely influenced by two atmospheric centers of
435 action: the Beaufort High and the Aleutian Low. The former is a quasi-stationary region of high
436 pressure located over the Beaufort Sea / Canada Basin, while the latter is the integrated signal of
437 individual storms progressing from west to east along the North Pacific storm track. Using the
438 NARR data, we averaged the sea level pressure (SLP) and 10 m wind fields for the upwelling and
439 non-upwelling periods (Fig. 13). For the upwelling composite, the Beaufort High is well devel-
440 oped north of Chukchi Sea, and there is a clear signature of the Aleutian Low centered over the
441 eastern Bering Sea and Alaskan portion of North America (Fig. 13a). As a result, strong north-
442 easterly winds are present throughout the Chukchi Sea, including Barrow Canyon, supported by
443 the gradient in SLP between the two centers of action. By contrast, in the non-forced composite
444 there is only a very weak signature of the Beaufort High and Aleutian Low (which are displaced to
445 the east and west, respectively, Fig. 13b). In this case the winds are light in Barrow Canyon. These
446 findings are consistent with Weingartner et al. (in press) who investigated aspects of upwelling in
447 Barrow Canyon using mooring data.

448 In order to further understand the impact of atmospheric systems on the upwelling, we tracked
449 the centers of all of the storms within the domain of Fig. 13 during the study period. The tracking

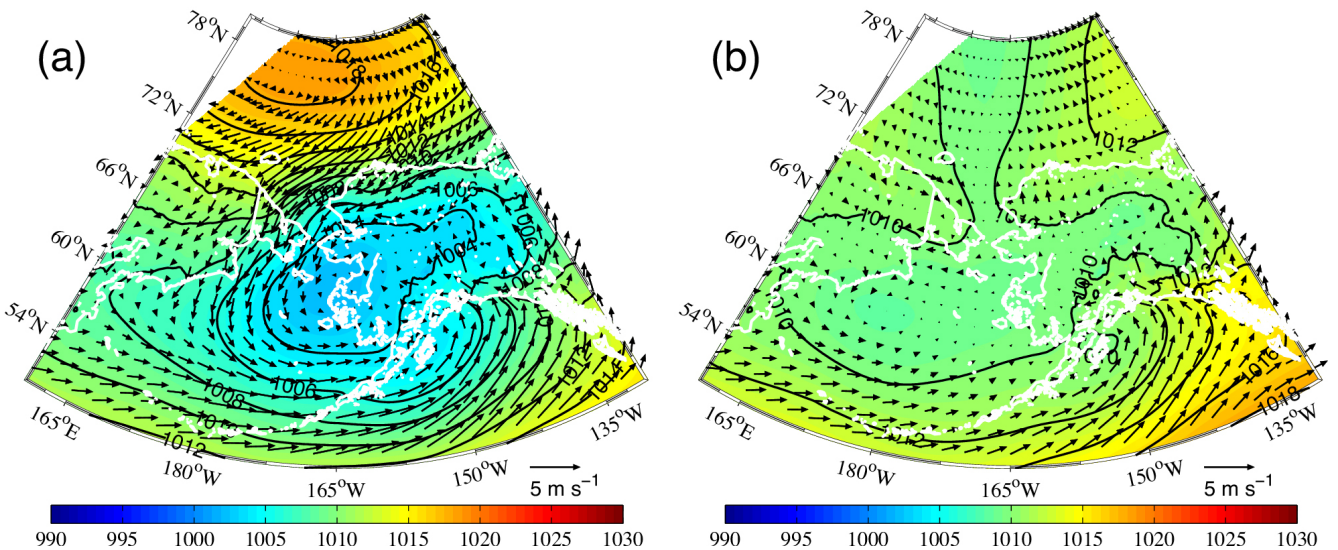


Figure 13: Composites of sea level pressure (color, mb) and 10 m wind (vectors, m/s) from NARR for (a) upwelling, and (b) non-upwelling periods.

450 was carried out visually using a graphical user interface (GUI) applied to the 6-hourly NARR
 451 fields. This technique has been used successfully in previous studies (e.g., Våge et al., 2008;
 452 Pickart et al., 2009a). One of the main advantages of manual storm tracking, versus automated
 453 methods, is that there is little to no ambiguity regarding the merging and splitting of storms. Using
 454 data for fall/winter 2002–3, Pickart et al. (2009b) showed that storms in this region that veer to
 455 the north and progress beyond roughly 65°N tend to cause upwelling in the Alaskan Beaufort Sea.
 456 This motivates us to consider if there are there similar trends for the Barrow Canyon region during
 457 the summer and early-fall.

458 Based on our calculated storm tracks, we divided the domain into a northern region (north of
 459 62°N), a southwest region (west of 165°W), and a southeast region (east of 165°W). In Figure 14
 460 we show two dominant types of storm tracks: those that end up in the northern region (Fig. 14a),
 461 and those that end up in the southeast region (Fig. 14b). In the figure, the red asterisk denotes
 462 where the storm was first identified in the study domain. In the first scenario, the storms either
 463 entered the northern region from the west or progressed into that region from the southwest region.
 464 In the second case, the storms entered the southeast region either from farther south or progressed

465 into that area from the southwest region. We refer to these two sets of storm tracks as mode 1 and
466 mode 2, respectively. Together, the two modes account for more than two-thirds of the storms.
467 Overall, there were 64 mode 1 storms and 63 mode 2 storms.

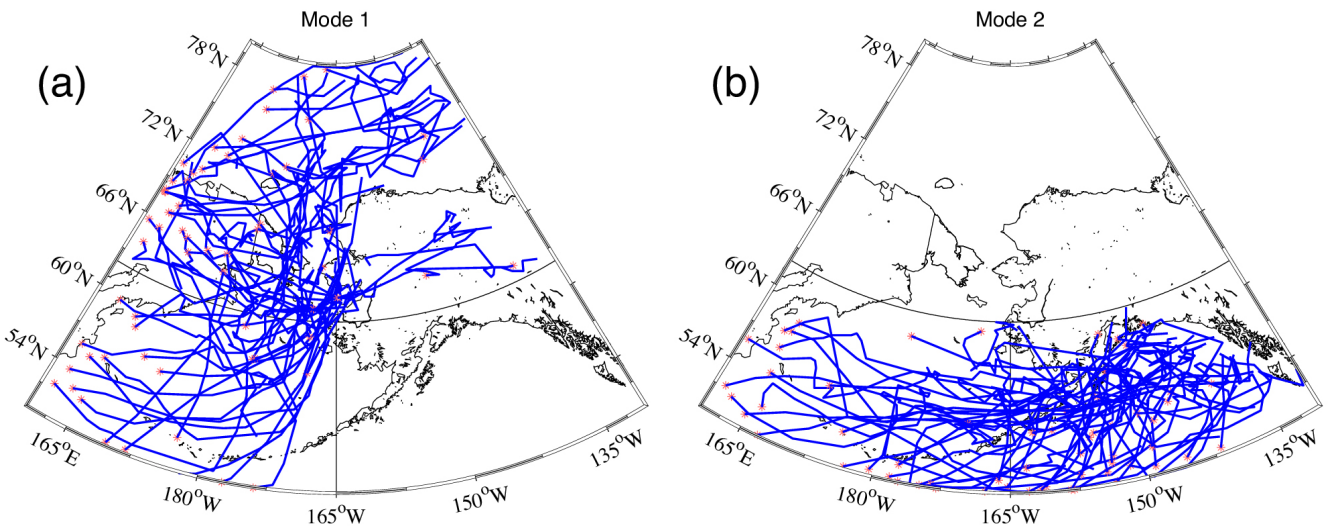


Figure 14: Two dominant modes of storm tracks during the study period. (a) mode 1; (b) mode 2. The three sub-regions discussed in the text are marked by black lines.

468 There is a clear seasonality associated with the two modes. Mode 1 storms are more frequent
469 in summer and decrease in occurrence through the early fall (Fig. 15a). Conversely, mode 2 storms
470 are less common in summer and occur more often in the later months. Using the Barrow timeseries,
471 we identified the parent storm that resulted in each of the upwelling events and tabulated where
472 the storm in question was located during the period of enhanced winds in Barrow Canyon. This
473 revealed that roughly half of the storms caused upwelling: 45% of the mode 1 storms and 55% of
474 the mode 2 storms. The seasonality of occurrence of these two subsets is the same as for the full
475 set of storms. Hence, mode 1 storms generally induce upwelling in summer, while mode 2 storms
476 induce upwelling in early-fall.

477 To determine the canonical upwelling conditions for each mode, we composited the SLP and
478 10 m wind for the segments of tracks associated with enhanced winds in Barrow Canyon for the
479 two cases. For mode 1, the composite reveals a well-developed Beaufort High and Aleutian Low,
480 with the latter centered in the northeast Bering Sea (Fig. 16a). The analogous composite for mode

481 2 also shows a well-developed Beaufort High and Aleutian Low, except in this case both of the
 482 centers of action are stronger and the Aleutian Low is now centered more to the southeast near the
 483 Alaskan Peninsula. In both instances the northeasterly winds in Barrow Canyon are comparable.
 484 The difference in the position of the Aleutian Low between the two composites is of course due to
 485 the difference in character of the storm tracks in mode 1 versus mode 2 (Fig. 14). We now consider
 486 the reasons behind the different types of modes.

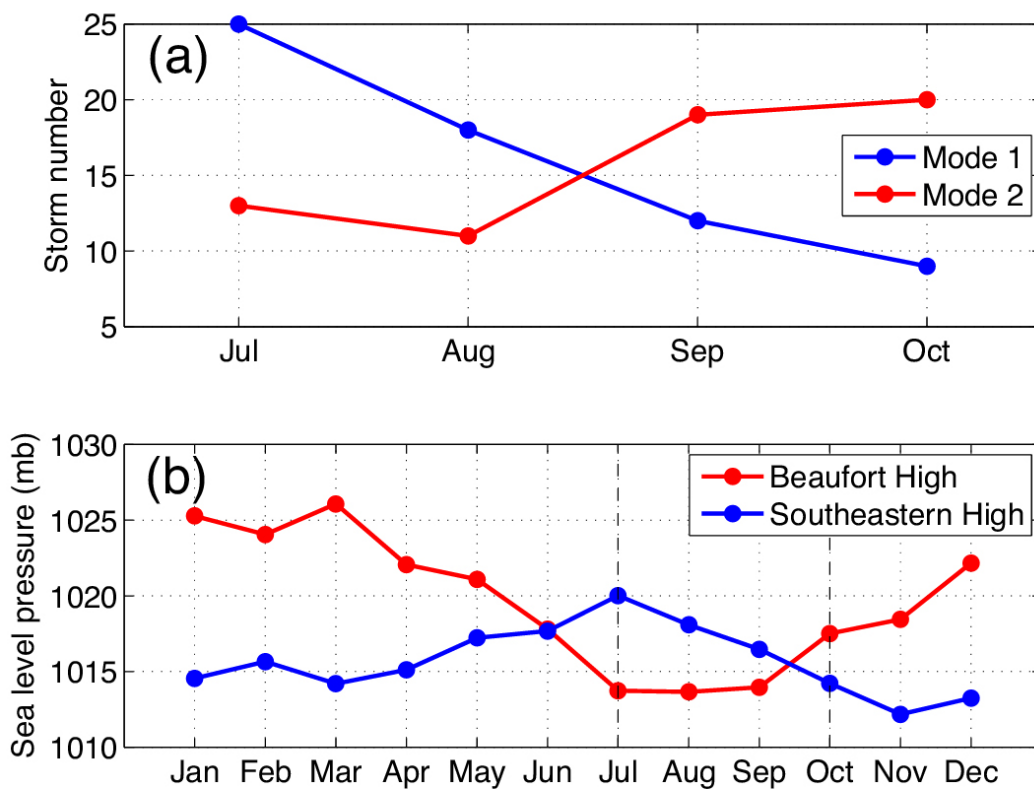


Figure 15: (a) Monthly occurrence of the two storm track modes during the study period. (b) Climatological monthly values of the Beaufort High and Southeastern High for the period 2000–2014 from NARR.

487 In addition to the strong Beaufort High in the mode 2 composite (Fig. 16b), note the presence
 488 of high SLP in the southeastern part of the domain in the mode 1 composite (16a). We refer to
 489 this latter feature as the “Southeastern High”. Pickart et al. (2009b) discussed the impact of high
 490 SLP blocking patterns in dictating the tracks of storms in their study of upwelling in the Beaufort
 491 Sea during fall/winter 2002–3. In light of that study, we considered the behavior of the Beaufort

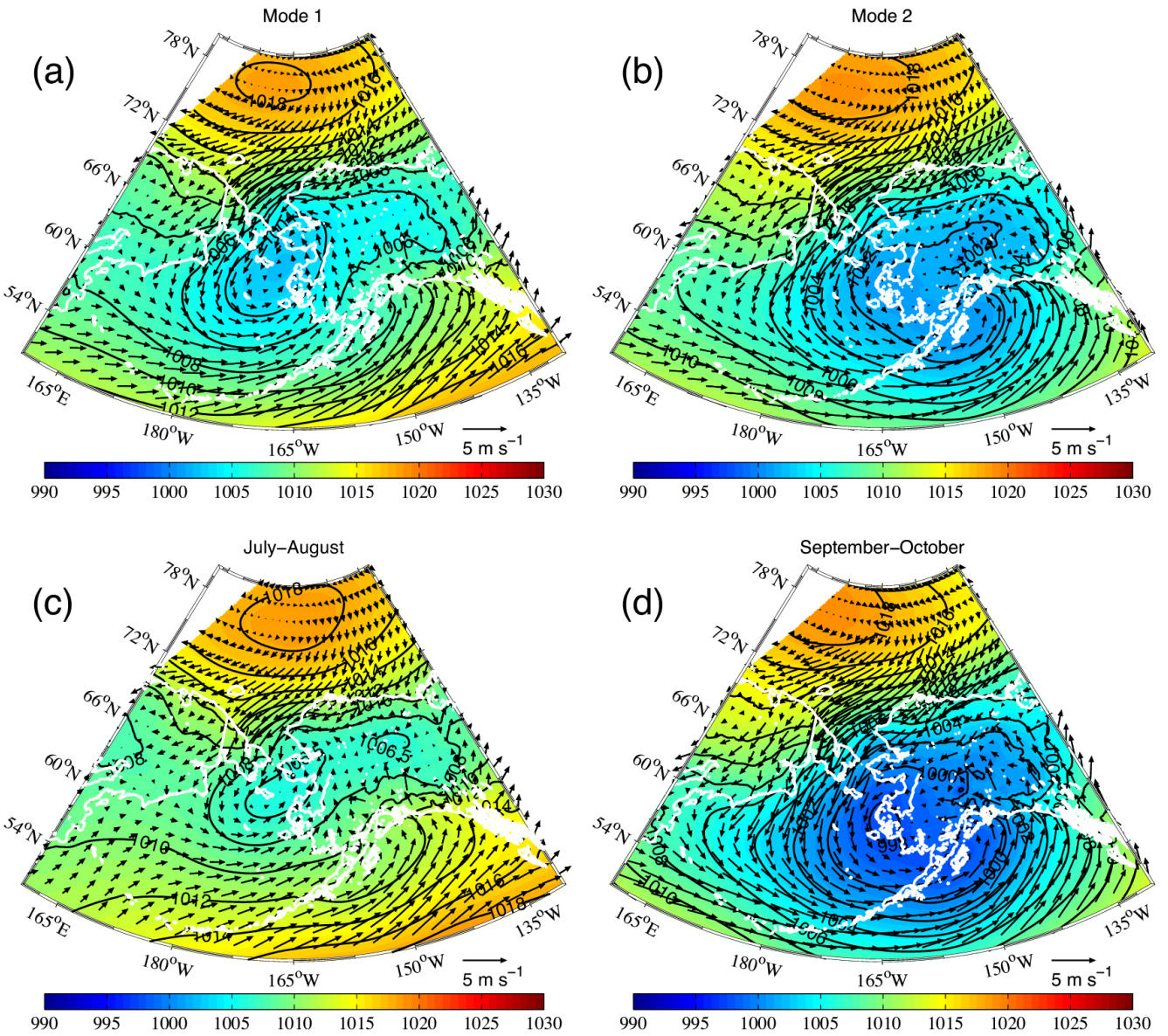


Figure 16: (a) Composite SLP and 10 m wind from NARR during upwelling periods of mode 1 storms. (b) same as (a) for mode 2 storms. (c) Composite SLP and 10 m wind from NARR for all upwelling periods in July–August. (d) same as (c) for September–October.

492 High and Southeastern High in our data set by constructing climatological monthly mean values of
493 these two centers of action over the full year (Figure 15b). (We considered the time period 2000–
494 2014 in order to make the monthly means more robust.) One sees that their magnitudes are out
495 of phase. Note in particular that the Southeastern High is strongest in summer, while the Beaufort
496 High is weakest that time of year. Furthermore, during the four-month period considered in our
497 study (July–October), there is a transition whereby the Southeastern High dominates early in the
498 period and the Beaufort High dominates later. This is in line with the variation in occurrence of
499 the two storm track modes (Figure 15a). The conclusion then is that a blocking Southeastern High
500 causes storms to veer northward (mode 1), while a blocking Beaufort High keeps the storms at a
501 more southerly latitude (mode 2).

502 Recall that the seasonality in occurrence for the subset of storms that result in upwelling is
503 similar to that for the entire set of storms shown in Figure 15a. As such, we compared the com-
504 posites of SLP and 10 m wind during times of upwelling in summer (July–August) and early-fall
505 (September–October). Notably, the former is close to the composite for mode 1 upwelling storms
506 (compare Fig. 16a and c), and the latter is similar to the composite for mode 2 upwelling storms
507 (compare Fig. 16b and d). This strengthens our interpretation that upwelling is primarily induced
508 by mode 1 storms in summer, when the Southeastern High is intensified and acts as a block, in
509 contrast to early fall when mode 2 storms cause upwelling, associated with a blocking Beaufort
510 High.

511 **4. Summary**

512 This study used a collection of 24 hydrographic transects occupied across Barrow Canyon
513 between 2010 and 2013 to study the seasonal evolution of water masses in the canyon from July–
514 October as well as the occurrence of upwelling. The sections were carried out as part of the
515 Distributed Biological Observatory (DBO) program, an international effort to obtain timeseries
516 at key locations in the western Arctic. The mean summer/early-fall sections revealed that the
517 Alaskan coastal water (ACW) is mainly confined to the eastern flank of the canyon, corresponding
518 to a region of sloped isopycnals indicative of the surface-intensified Alaskan Coastal Current. The

519 Pacific-origin winter water is found at depth, banked against the western flank of the canyon. The
520 isopycnal structure in this region is consistent with a bottom-intensified flow of this dense water
521 mass out of the canyon.

522 All of the Pacific-origin water masses were present in the canyon at some point during the
523 four-month period. The most prominent water mass was the winter water, which is subdivided into
524 very cold newly ventilated winter water (NVWW) and warmer remnant winter water (RWW). The
525 NVWW appeared almost exclusively in August, which is consistent with earlier studies showing
526 that this water mass is carried across the Chukchi Shelf via interior pathways. Our results suggest
527 that these pathways deliver the dense winter water to Barrow Canyon within a month-long window
528 in late summer. The next most prominent water mass was Bering summer water (BSW) which was
529 measured during each month of the study period. The ACW had its maximum presence in August
530 and September. Our analysis indicates that this water mass is converted to a relatively warm, fresh
531 variety of BSW in October,

532 Roughly a third of the hydrographic sections were preceded by significant up-canyon winds
533 and were categorized as under the influence of upwelling. The composite average of these cases,
534 compared to the non-forced realizations, revealed that anomalously salty water is found throughout
535 the eastern flank of the canyon during upwelling. At the base of the canyon the water is warmer
536 than average, while near the shelfbreak the water is colder than average. This reflects the fact that
537 warm, salty Atlantic water (AW) is occasionally upwelled into the canyon, while the colder Pacific-
538 origin winter waters that normally occupy the deepest part of the canyon are drawn to shallower
539 depths. The only time that AW was measured in the canyon was during such wind events, at which
540 time ACW was absent from the canyon. Our data indicate that the conversion of ACW to BSW
541 occurs via wind mixing during the upwelling.

542 Using reanalysis fields we characterized the atmospheric circulation associated with upwelling
543 in the canyon during the four month study period. To get a larger sample size we used the Barrow
544 wind data to identify likely upwelling events using a similar criteria as that applied to the hydro-
545 graphic sections. Consistent with previous studies, we found that upwelling occurs in the canyon
546 when there is an enhanced Beaufort High north of the Chukchi Sea and a deep Aleutian Low in

547 the Bering Sea. To elucidate the nature of the atmospheric patterns, we tracked all of the storms
548 in the domain during the study period, which revealed that there are two dominant modes: one in
549 which the storms mainly progress to the north, and the other when they predominantly progress
550 to the east. The mode 1 storms are more common in the summer, while the mode 2 storms oc-
551 cur more frequently in the early-fall. Both types result in upwelling roughly half the time. Our
552 analysis suggests that the relative strength of the Beaufort High versus a region of high pressure
553 in the southeast part of the domain (referred to as the Southeastern High) dictate this seasonality.
554 In particular, in July–August the Southeastern High acts as a block which causes more storms to
555 progress northward, while in September–October the Beaufort High serves as a block and accord-
556 ingly storms tend to travel eastwards. Both scenarios appear to be equally effective for driving
557 upwelling in Barrow Canyon.

558 As the DBO program goes forward, and more sections are added to the timeseries, this will
559 allow us to further refine the seasonal patterns identified here, and give us the opportunity to in-
560 vestigate the interannual variability of the water masses and wind-forced conditions in Barrow
561 Canyon.

562 **5. Acknowledgements**

563 The authors are indebted to the officers and crew of the research vessels listed in Table 1 and to
564 the many technicians who helped collect and process the data used in the study. Funding for the US
565 component of DBO was provided by the National Science Foundation under grants ARC-1203906,
566 ARC-1204044, ARC-1204082, PLR-1023331.

567 **References**

- 568 K. Aagaard and A. T. Roach. Arctic ocean-shelf exchange: Measurements in Barrow Canyon.
569 *Journal of Geophysical Research*, 95:18,163–18,175, 1990.
- 570 R. H. Bourke and R. G. Paquette. Atlantic water on the Chukchi shelf. *Geophysical Research*
571 *Letters*, 3:629–632, 1976.

- 572 E. T. Brugler. Interannual variability of the Pacific water boundary current in the Beaufort Sea.
573 Master's thesis, Massachusetts Institute of Technology and Woods Hole Oceanographic Institu-
574 tion, Cambridge/Woods Hole, WA, 2013. 120 pp.
- 575 E. T. Brugler, R. S. Pickart, G. W. K. Moore, S. Roberts, T. J. Weingartner, and H. Statscewich.
576 Seasonal to interannual variability of the Pacific water boundary current in the Beaufort Sea.
577 *Progress in Oceanography*, 127:1–20, 2014.
- 578 L. Cooper, K. Frey, C. Logvinova, D. Biasatti, and J. Grebmeier. Variations in the proportions
579 of melted sea ice and runoff in surface waters of the Chukchi Sea: A retrospective analysis,
580 1990-2012, and analysis of the implications of melted sea ice in an under-ice bloom. *Deep Sea*
581 *Research II*, 130:6–13, 2016.
- 582 W. Corlett and R. S. Pickart. The chukchi slope current. *Progress in Oceanography*, 153:50–56,
583 2017.
- 584 E. D'Asaro. Generation of submesoscale vortices: A new mechanism. *Journal of Geophysical*
585 *Research*, 93:6685–6693, 1988.
- 586 D. Gong and R. S. Pickart. Summertime circulation in the eastern Chukchi Sea. *Deep Sea Research*
587 *II*, 118:18–31, 2015.
- 588 D. Gong and R. S. Pickart. Early summer water mass transformation in the eastern Chukchi Sea.
589 *Deep Sea Research II*, 130:43–55, 2016.
- 590 M. Gonsior, J. Luek, P. Schmitt-Kopplin, J. Grebmeier, and L. Cooper. Optical properties and
591 molecular diversity of dissolved organic matter in the Bering Strait and Chukchi Sea. *Deep Sea*
592 *Research II*, page <https://doi.org/10.1016/j.dsr2.2017.01.003>, 2017.
- 593 J. Grebmeier, S. Moore, J. Overland, K. Frey, and R. Gradinger. Biological response to recent
594 Pacific Arctic sea ice retreats. *EOS, Transactions, American Geophysical Union*, 91:161–162,
595 2010.

- 596 V. Hill, G. Cota, and D. Stockwell. Spring and summer phytoplankton communities in the Chukchi
597 and eastern Beaufort Seas. *Deep Sea Research II*, 52:3369–3385, 2005.
- 598 A. Huyer, E. Sobey, and R. Smith. The spring transition in currents over the Oregon continental
599 shelf. *Journal of Geophysical Research*, 84:6995–7011, 1979.
- 600 M. Itoh, K. Shimada, T. K. and F. McLaughlin, E. Carmack, and S. Nishino. Inter-annual vari-
601 ability of Pacific winter water inflow through Barrow Canyon from 2000 to 2006. *Journal of*
602 *Oceanography*, 68:575–592, 2012.
- 603 M. Itoh, S. Nishino, Y. Kawaguchi, and T. Kikuchi. Barrow Canyon volume, heat, and fresh-
604 water fluxes revealed by long-term mooring observations between 2000 and 2008. *Journal of*
605 *Geophysical Research*, 118:1–17, 2013.
- 606 M. Itoh, R. S. Pickart, T. Kikuchi, Y. Fukamachi, K. I. Ohshima, D. Simizu, K. R. Arrigo, S. Vagle,
607 J. He, C. Ashjian, J. T. Mathis, S. Nishino, and C. Nobre. Water properties, heat and volume
608 fluxes of Pacific water in Barrow Canyon during summer 2010. *Deep Sea Research I*, 102:
609 43–54, 2015.
- 610 C. Ladd, C. W. Mordy, S. A. Salo, and P. J. Stabeno. Winter water properties and the Chukchi
611 polynya. *Journal of Geophysical Research*, 121:5516–5534, 2016.
- 612 P. Lin, R. Pickart, K. Stafford, G. Moore, D. Torres, F. Bahr, and J. Hu. Seasonal variation of the
613 Beaufort shelfbreak jet and its relationship to Arctic cetecean occurrence. *Journal of Geophys-
614 ical Research*, 121:doi:10.1002/2016JC011890, 2016.
- 615 K. Lowry, R. Pickart, M. Mills, Z. Brown, G. van Dijken, N. Bates, and K. Arrigo. Influence of
616 winter water on phytoplankton blooms in the Chukchi Sea. *Deep Sea Research II*, 118:53–72,
617 2015.
- 618 D. G. Mountain, L. K. Coachman, and K. Aagaard. On the flow through Barrow Canyon. *Journal*
619 *of Physical Oceanography*, 6:461–470, 1976.

- 620 R. D. Muench, J. D. Schumacher, and S. A. Salo. Winter currents and hydrographic conditions on
621 the northern central Bering Sea shelf. *Journal of Geophysical Research*, 93:516–526, 1988.
- 622 A. Nikolopoulos, R. S. Pickart, P. S. Fratantoni, K. Shimada, D. J. Torres, and E. P. Jones. The
623 western arctic boundary current at 152°W: Structure, variability, and transport. *Deep Sea Re-*
624 *search II*, 56:1164–1181, 2009.
- 625 S. Okkonen, C. Ashjian, R. Campbell, W. Maslowski, J. Clement-Kinney, and R. Potter. Intrusion
626 of warm Bering/Chukchi waters onto the shelf in the western Beaufort Sea. *Journal of*
627 *Geophysical Research*, 114:doi:10.1029/2008JC004870, 2009.
- 628 A. Pacini, R. Pickart, G. Moore, C. Nobre, F. Bahr, K. Vage, and K. Arrigo. Characteristics and
629 transformation of pacific winter water on the chukchi sea shelf in late-spring. *Deep Sea Research*
630 *II*, this issue.
- 631 R. Pickart, L. M. Schulze, G. W. K. Moore, M. A. Charette, K. R. Arrigo, G. van Dijken, and S. L.
632 Danielson. Long-term trends of upwelling and impacts on primary productivity in the Beaufort
633 Sea. *Deep Sea Research I*, 79:106–121, 2013.
- 634 R. Pickart, G. Moore, C. Mao, F. Bahr, C. Nobre, and T. Weingartner. Circulation of winter water
635 on the Chukchi shelf in early summer. *Deep Sea Research II*, 130:56–75, 2016.
- 636 R. S. Pickart and G. Stossmeister. Outflow of Pacific water from the Chukchi sea to the Arctic
637 Ocean. *Chinese Journal of Polar Oceanography*, 10:135–148, 2008.
- 638 R. S. Pickart, D. J. Torres, and P. S. Fratantoni. The east Greenland spill jet. *Journal of Physical*
639 *Oceanography*, 35:1037–1053, 2005.
- 640 R. S. Pickart, G. W. K. Moore, A. M. Macdonald, I. A. Renfrew, J. E. Walsh, and W. S. Kessler.
641 Seasonal evolution of Aleutian low-pressure systems: Implications for the North Pacific sub-
642 polar circulation. *Journal of Physical Oceanography*, 39:1316–1339, 2009a.

643 R. S. Pickart, G. W. K. Moore, D. J. Torres, P. S. Fratantoni, R. A. Goldsmith, and J. Yang.
644 Upwelling on the continental slope of the Alaskan Beaufort Sea: Storms, ice, and oceanographic
645 response. *Journal of Geophysical Research*, 114:C00A13, doi:10.1029/2208JC005009, 2009b.

646 R. S. Pickart, L. J. Pratt, D. J. Torres, T. E. Whitledge, A. Y. Proshutinsky, K. Aagaard, T. A.
647 Agnew, G. W. K. Moore, and H. J. Dail. Evolution and dynamics of the flow through Herald
648 Canyon in the western Chukchi Sea. *Deep Sea Research II*, 57:5–26, 2010.

649 R. S. Pickart, M. A. Spall, G. W. K. Moore, T. J. Weingartner, R. A. Woodgate, K. Aagaard, and
650 K. Shimada. Upwelling in the Alaskan Beaufort Sea: Atmospheric forcing and local versus
651 non-local response. *Progress in Oceanography*, 88:78–100, doi:10.1016/j.pocean.2010.11.005,
652 2011.

653 M. Pisareva, R. Pickart, M. Spall, C. Nobre, D. Torres, and G. Moore. Flow of pacific water in the
654 western Chukchi Sea: Results from the 2009 RUSALCA expedition. *Deep Sea Research I*, 105:
655 53–73, 2015.

656 M. Pisareva, R. Pickart, P. Fratantoni, and T. Weingartner. On the nature of wind-forced upwelling
657 in Barrow Canyon. *Deep Sea Research II*, this issue.

658 L. M. Schulze and R. S. Pickart. Seasonal variation of upwelling in the Alaskan Beaufort Sea:
659 Impact of sea ice cover. *Journal of Geophysical Research*, 100:in press, 2012.

660 K. Shimada, E. Carmack, K. Hatakeyama, and T. Takizawa. Varieties of shallow temperature
661 maximum waters in the western Canadian Basin of the Arctic Ocean. *Geophysical Research*
662 *Letters*, 28:3441–3444, 2001.

663 E. Shroyer and R. Pickart. Pathways, timing, and evolution of Pacific winter water through Barrow
664 Canyon. *Deep Sea Research II*, this issue.

665 E. Shroyer and A. Pleuddemann. Wind-driven modification of the Alaska coastal current. *Journal*
666 *of Geophysical Research*, 117:doi:10.1029/2011JC007650, 2012.

- 667 S. Signorini, A. Munchow, and D. Haidvogel. Flow dynamics of a wide Arctic canyon. *Journal of*
668 *Geophysical Research*, 102:18,661–18,680, 1997.
- 669 M. A. Spall. Circulation and water mass transformation in a model of the Chukchi Sea. *Journal of*
670 *Geophysical Research*, 112:C05025, doi:10.1029/2005JC003364, 2007.
- 671 K. Våge, R. S. Pickart, G. W. K. Moore, and M. H. Ribergaard. Winter mixed-layer development
672 in the central Irminger Sea: The effect of strong, intermittent wind events. *Journal of Physical*
673 *Oceanography*, 38:541–565, 2008.
- 674 W.-J. von Appen and R. S. Pickart. Two configurations of the western Arctic shelfbreak current in
675 summer. *Journal of Physical Oceanography*, 42:329–351, 2012.
- 676 T. J. Weingartner, D. J. Cavalieri, K. Aagaard, and Y. Sasaki. Circulation, dense water formation,
677 and outflow on the northeast chukchi shelf. *Journal of Geophysical Research*, 103:7647–7661,
678 1998.
- 679 T. J. Weingartner, K. Aagaard, R. Woodgate, S. Danielson, Y. Sasaki, and D. Cavalieri. Circulation
680 on the north central Chukchi Sea shelf. *Deep Sea Research II*, 52:3150–3174, 2005.
- 681 T. J. Weingartner, E. Dobbins, S. Danielson, P. Winsor, R. Potter, and H. Statscewich. Hydro-
682 graphic variability over the northeastern Chukchi Sea shelf in summer-fall 2008-2010. *Conti-*
683 *ental Shelf Research*, 67:5–22, 2013.
- 684 T. J. Weingartner, E. Dobbins, S. Danielson, P. Winsor, R. Potter, and H. Statscewich. Hydro-
685 graphic variability over the northeastern Chukchi Sea shelf in summer-fall 2008-2010. *Deep*
686 *Sea Research*, in press.
- 687 P. Winsor and D. Chapman. Pathways of pacific water across the Chukchi Sea: a numerical model
688 study. *Journal of Geophysical Research*, 109:http://dx.doi.org/10.1029/2003JC001962, 2004.
- 689 R. A. Woodgate, K. Aagaard, and T. J. Weingartner. Monthly temperature, salinity, and trans-
690 port variability of the Bering Strait throughflow. *Geophysical Research Letters*, 32:L04601,
691 doi:10.1029/2004GL021880, 2005.

692 R. A. Woodgate, K. Stafford, and F. Prah. A synthesis of year-round interdisciplinary mooring
693 measurements in the Bering Strait (1990–2014) and the RUSALCA years (2004–2011).
694 *Oceanography*, 28:46–67, 2015.